Inorganic Chemistry

pubs.acs.org/IC Article

Solution Chemistry of Copper(II) Binding to Substituted 8-Hydroxyquinolines

Kelly L. Summers,* M. Jake Pushie, George J. Sopasis, Ashley K. James, Natalia V. Dolgova, Dimosthenis Sokaras, Thomas Kroll, Hugh H. Harris, Ingrid J. Pickering,* and Graham N. George*

Cite This: https://dx.doi.org/10.1021/acs.inorgchem.0c01356 Read Online

ACCESS | Metrics & More | Article Recommendations | Supporting Information

ABSTRACT: 8-Hydroxyquinolines (8HQs) are a family of lipophilic metal ion chelators that have been used in a range of analytical and pharmaceutical applications over the last 100 years. More recently, CQ (clioquinol; 5-chloro-7-iodo-8-hydroxyquinoline) and PBT2 (5,7-dichloro-2-[(dimethylamino)methyl]-8-hydroxyquinoline) have undergone clinical trials for the treatment of Alzheimer's disease and Huntington's disease. Because CQ and PBT2 appear to redistribute metals into cells, these compounds have been redefined as copper and zinc ionophores. Despite the attention surrounding the clinical trials and the clear link between 8HQs and metals, the fundamental solution chemistry of how these compounds bind divalent metals such as copper and zinc, as well as their mechanism(s) of action in mammalian systems, remains poorly understood. In this study, we used a combination of X-ray absorption spectroscopy (XAS), high-energy resolution fluorescence detected (HERFD) XAS, electron paramagnetic resonance (EPR), and UV−visible absorption spectroscopies to investigate the aqueous solution chemistry of a range of 8HQ derivatives. To circumvent the known solubility issues with 8HQ compounds and their complexes with Cu(II), and to avoid the use of abiological organic solvents, we have devised a surfactant buffer system to investigate these Cu(II) complexes in aqueous solution. Our study comprises the first comprehensive investigation of the Cu(II) complexes formed with many 8HQs of interest in aqueous solution, and it provides the first structural information on some of these complexes. We find that halogen substitutions in 8HQ derivatives appear to have little effect on the Cu(II) coordination environment; 5,7-dihalogenated 8HQ conformers all have a pseudo square planar Cu(II) bound by two quinolin-8-olate anions, in agreement with previous studies. Conversely, substituents in the 2-position of the 8HQ moiety appear to cause significant distortions from the typical square-planar-like coordination of most Cu(II)-bis-8HQ complexes, such that the 8HQ moieties in the Cu(II)-bis-8HQ complex are rotated approximately 30−40° apart in a "propeller-like" arrangement.

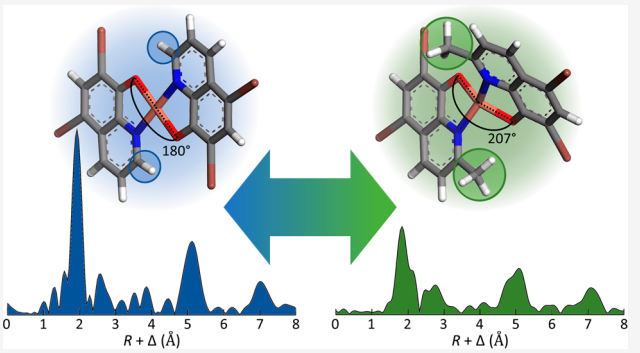

1. INTRODUCTION

First prepared by Skraup, Bedall, and Fischer in the early 1870s,[1] 8-hydroxyquinoline (8HQ) and its derivatives comprise a family of lipophilic metal ion chelators that have been used in a range of applications from laboratory-based techniques to medications over the last century. For example, 8HQs have been used extensively since the 1920s as gravimetric and colorimetric analytical reagents for transition metals.[1−4] 8-Hydroxyquinoline (oxine; 8HQ), as well as many of its derivatives (Figure 1), including dihalogenated 5,7-dibromo-8-hydroxiquinoline (bromoxine; B2Q),[5] 5,7-dichloro-8-hydroxiquinoline (chloroxine; Cl2Q),[6] and 5,7-diiodo-8-hydroxiquinoline (iodoxine; I2Q),[7] have been used for this purpose.

8HQs have also been used as antiseptics, disinfectants, pesticides, and antifungal and antiprotozoal drugs since the 1930s.[1,8−10] For example, clioquinol (5-chloro-7-iodo-8-hydroxyquinoline; iodochlorhydroxyquin; CQ) was marketed as an over-the-counter antidiarrheal medication until all halogenated 8HQs were withdrawn as medications in Japan in 1970,[11] and all oral preparations were discontinued worldwide by 1985.[12] However, a small number of topical ointments remain available in some countries (e.g., Dermasorb in the United States and Vioform in Canada). CQ use significantly declined when it was linked to an outbreak of subacute myelo-optic neuropathy (SMON) in Japan from 1955 to 1970. Over 10,000 SMON cases were reported, with neurological symptoms including blindness, lower limb spasticity, and sensory dysfunction.[13,14] Many people were

Received: May 8, 2020

https://dx.doi.org/10.1021/acs.inorgchem.0c01356
Inorg. Chem. XXXX, XXX, XXX−XXX

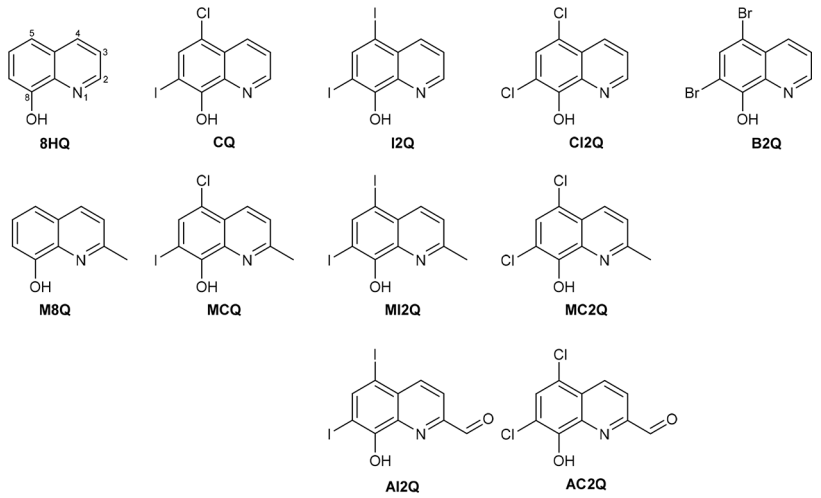

Figure 1. Schematic structures of 8-hydroxyquinoline (showing ring numbering) and 8-hydroxyquinoline derivative compounds studied herein. See text for full chemical names.

permanently disabled.[13] The exact cause of SMON is still debated; however, excessive consumption of CQ[14] (up to 4 g/day in one case[15]) is thought to induce dyshomeostasis or deficiency of essential metals like copper, zinc, or iron—especially if CQ is taken with iron supplements—and to result in SMON-like symptoms.[8,16−19] Prior to the SMON outbreak, CQ was not thought to be absorbed from the gastrointestinal (GI) tract, but the neurodegenerative symptoms of SMON, as well as isolation of CQ compounds in urine,[20] suggest that CQ is indeed absorbed through the GI tract and crosses the blood-brain barrier.

The potential role of CQ in SMON has raised some concerns more recently as CQ and PBT2 (5,7-dichloro-2-[(dimethylamino)methyl]-8-hydroxyquinoline) have gained attention as candidate drugs for the treatment of some neurological diseases (e.g., Alzheimer's disease and Huntington's disease) and cancers. Preclinical studies of CQ in Alzheimer's model animals showed promising results including decreased amyloid plaque burden and improved memory.[21,22] Similarly, improvements in memory and cognition were reported from a phase II clinical trial[23] and a case study[24] on Alzheimer's disease (AD) patients. Despite these promising results from animal studies[21] and clinical trials,[23] contamination in large-scale synthesis of CQ halted further testing as an AD treatment.[22] Following this issue with CQ synthesis, PBT2 was designed as a second generation anti-AD 8HQ analogue with improved solubility. PBT2 showed greater therapeutic potential than CQ in an AD mouse model[22] and in a phase II clinical trial.[25,26] Results from the most recent extended clinical trial investigating the anti-AD properties of PBT2 in patients are yet to be published; however, PBT2 was reported to have no significant effect on amyloid burden compared to placebo patients,[27] contrary to results from earlier phase II trials.[25] Importantly, no adverse effects of CQ or PBT2 treatment, such as those observed in SMON, were reported in animals or patients in these studies.[21−23,25,26]

PBT2 and CQ were also evaluated for the treatment of Huntington's disease (HD). Similar to AD, HD is a progressive neurodegenerative disease characterized by cell loss and atrophy, as well as aggregation of mutant huntingtin protein.[28] Studies of CQ in animal models of HD noted improved behavioral and pathologic phenotypes, including decreased huntingtin aggregate accumulation.[29] CQ was abandoned as a potential treatment in HD, as it was in AD, because of the difficulties associated with large-scale synthesis. However, PBT2 was subsequently tested in animal models of HD and was found to have similar positive outcomes to its predecessor.[30] In addition, PBT2 was shown to improve cognition, particularly executive function, and reduce brain atrophy in HD clinical trials.[31,32] PBT2 was presumed to act similarly to CQ, through inhibition of copper interactions with the HD-causing huntingtin protein in the brain.[29]

In addition to their anti-AD and anti-HD properties, 8HQs have also been shown to have potential anticancer properties. Specifically, 8HQs have been found to inhibit cancer cell growth and damage DNA when bound to iron;[33] some zinc- and copper-bound 8HQs were found to interact with DNA, likely through intercalation and electrostatic interactions.[34] Similarly, 8HQs recently have been shown to inhibit the activity of a transcription factor important for cancer cell survival; 8HQs are thought to bind to the active site through coordination of the Fe(II) ion and thereby inhibit the binding of a key cosubstrate.[35] DNA intercalation and damage, as well as protein inhibition, by metal-bound 8HQs may point to metal-triggered anticancer mechanism(s) of action for these metal 8HQ complexes.

Because CQ and PBT2 appear to redistribute metals into cells, these compounds have more recently been characterized as copper and zinc ionophores.[36−39] In AD, copper and zinc redistribution into deficient neurons is thought to trigger a signaling pathway that results in reduced amyloid β levels in the brain and improved cognition.[38,40] In cancers, redistribution of copper, zinc, and iron into cancer cells is thought to trigger toxic metal ion accumulation, which then results in cancer cell death.[39,41−44] In addition, this ionophoric character of 8HQs may explain the effectiveness of 8HQ treatment in other metal-linked diseases such as acrodermatitis enteropathica, a lethal inherited human zinc-deficiency disorder.[45−47]

Although the many beneficial properties of this family of drug compounds have been exploited for about 100 years, the fundamental solution chemistry of how these compounds bind divalent metals such as copper and zinc, as well as their mechanism(s) of action in mammalian systems, remains poorly understood. 8-Hydroxyquinoline compounds and their Cu(II) complexes are highly hydrophobic, with a number of solubility

https://dx.doi.org/10.1021/acs.inorgchem.0c01356
Inorg. Chem. XXXX, XXX, XXX−XXX

issues and precipitate formation reported in many previous studies,[2,3,41,48−52] which makes aqueous solution studies particularly difficult. As a result of this low solubility, nearly all experimental work reported to date on such complexes has used powders, crystals, or abiological solvents such as dimethyl sulfoxide (DMSO), dimethylformamide (DMF), or toluene. Structurally, 8HQs are generally thought to bind Zn(II) and Cu(II) in an 8HQ/M^{2+} ratio of 2:1 through bidentate chelation to the oxygen and nitrogen ligands. The structure of Cu(II)-CQ has been investigated previously by X-ray crystallography,[53] and by X-ray absorption spectroscopy (XAS) by others,[54] as well as by our group.[55] From the crystal structure it was evident that 2 CQ molecules coordinate Cu(II) through phenolate and nitrogen donors in a square-planar type geometry.[53] Surprisingly, previous XAS by Chen et al.[54] reported an octahedral copper coordination environment for CQ with six oxygen or nitrogen ligands. However, the oxidation state of the copper had been reduced from the initial Cu(II) state to a Cu(I) species, likely contributing to their contradictory conclusions.[54] XAS analysis of Cu(II) CQ solutions from our group has contested the analysis of Chen et al. and provided evidence for an approximately square planar Cu(II) species.[55]

The structure of the Cu(II) B2Q complex has also been studied previously by X-ray crystallography and found to be similar to that of Cu(II) CQ, including a square planar-like Cu(II) center in a coordination environment of two oxygen and two nitrogen atoms from two *trans*-quinolin-8-olate anions.[34] Early electron paramagnetic resonance (EPR) studies of powders and frozen solutions of B2Q, Cl2Q, and I2Q also suggest that the Cu(II) coordination environment of two oxygens and two nitrogens in a *trans* position is highly similar in these complexes and is therefore thought to be independent of halogen substitution.[56] More recent EPR analyses of frozen solutions appear similar to early studies.[48] Despite the structural characterizations described above, definitive aqueous solution structures are lacking for Cu(II) complexes of many of the 8HQs shown in Figure 1.

In this study, we used a combination of XAS, high-energy resolution fluorescence detected (HERFD) XAS, EPR, and UV−visible absorption spectroscopies to investigate the solution chemistry of a range of 8HQ derivatives (Figure 1). To circumvent the known solubility issues with 8HQ compounds and their complexes with Cu(II), and to avoid the use of various abiological solvents, we have devised a buffer system that includes a surfactant to allow us to probe these Cu(II) complexes in aqueous solution. As a result, our study provides a comprehensive examination of the aqueous solution chemistry of 8HQ complexes with Cu(II). To the best of our knowledge, for many 8HQs this is the first structural investigation of the Cu(II) complexes formed in aqueous solution, and for some, this study contains the only structural data available to date (e.g., MCQ, MI2Q, AI2Q, MC2Q, AC2Q; Figure 1). We find that halogen substitutions in the 5- and 7-positions of 8HQ derivatives appear to have little effect on the Cu(II) coordination environment; 5,7-dihalogenated 8HQ conformers all have a pseudo square planar type Cu(II) bound by two quinolin-8-olate anions, in agreement with previous studies.[34,53,55] Conversely, substituents in the 2-position of the 8HQ moiety appear to cause significant distortions from the typical pseudo square planar coordination of most Cu(II)-bis-8HQ complexes, such that the planes of the individual 8HQ ligands are no longer coplanar with each other and instead form a "propeller"-type arrangement. Because 8HQs are used to treat several diseases of metal ion dyshomeostasis, which often require compounds to cross the blood−brain barrier, the properties of 8HQs and their Cu(II) complexes (e.g., hydrophobicity, planarity, and Cu(II) coordination) may have a significant impact on their ability to reach the brain and restore metal ion homeostasis.

2. RESULTS AND DISCUSSION

Because 8-hydroxyquinoline compounds, and particularly their Cu(II) complexes, are highly hydrophobic, few studies have successfully investigated these complexes in aqueous solution. A number of solubility issues, including precipitate formation, has been reported in many previous studies,[2,3,41,48−52] in which investigations were often only performed on either the solvent solution fraction or the precipitate. To circumvent these issues with low solubility, most of the previous experimental work on 8HQ complexes has been conducted on powders, crystals, or in abiological solvents such as dimethyl sulfoxide (DMSO), dimethylformamide (DMF), or toluene. We devised a buffered surfactant solution (i.e., 400 mM dodecyl trimethylammonium bromide (DTAB) in 100 mM 3-(*N*-morpholino)-propanesulfonic acid (MOPS) at pH 7.4) that allowed us to examine the Cu(II) complexes of the 8HQs shown in Figure 1 in aqueous solution using several techniques. The results of hydrophobicity calculations and UV−visible absorption spectra can be found in the Supporting Information. We report results from geometry optimization calculations for the lowest energy structures of Cu(II) 8HQ complexes below before discussing the solution structure results from XAS, HERFD-XAS, and EPR.

2.1. Density Functional Theory Structure Calculations. The results of DFT calculations of Cu(II)-bis-I2Q and Cu(II)-bis-AI2Q complexes are shown in Figures 2 and S3. The DFT calculations show that Cu(II) coordination environments in which the two oxygen and two nitrogen ligands are in a *trans* arrangement are consistently lower in energy, compared with the *cis* configuration, by approximately 15−44 kJ/mol depending on the 8HQ (Table S2), which appears to agree with an early work by Palenik (1964)[57] and others.[56,58,59] The *trans* complexes formed with Cu(II) and 8HQs with 2-H substituents have C_{2h} point group symmetry such that all the atoms are in the same plane (the mirror plane), there is a center of inversion, and there is a 2-fold rotation axis at the Cu(II) center. The bond angles approach that expected for square planar geometry (i.e., 90.0°), with τ^4 and $\tau^{4\prime}$ parameter values of 0 (Figure 3; Table 1).[60,61] Interestingly, the *cis* configuration is approximately isoenergetic for Cu(II) complexes with AC2Q and AI2Q, unless the *trans* configuration is distorted such that the plane of one of the quinolin-8-olate anions is rotated approximately 40° from the plane defined by the other 8HQ ligand (Figure 2; Figure 3; Table 1). These distorted *trans* complexes have C_2 symmetry; there is no longer a mirror plane or a center of inversion, but there is still a 2-fold rotational axis at the Cu(II). The bond angle between the Cu(II)−O and the Cu(II)−N bond of the same 8HQ molecule (angle *x* in Figure 3) is constrained by the formation of a 5-membered chelate ring and therefore always remains within the narrow range of 83.4−84.5°, even after accounting for changes in the Cu−O and Cu−N bond distances. The bond angles between the Cu(II)−O and the Cu(II)−N bonds of different 8HQ molecules (angle *y* in Figure 3) are not similarly constrained and deviate appreciably from the 95.5−

https://dx.doi.org/10.1021/acs.inorgchem.0c01356
Inorg. Chem. XXXX, XXX, XXX−XXX

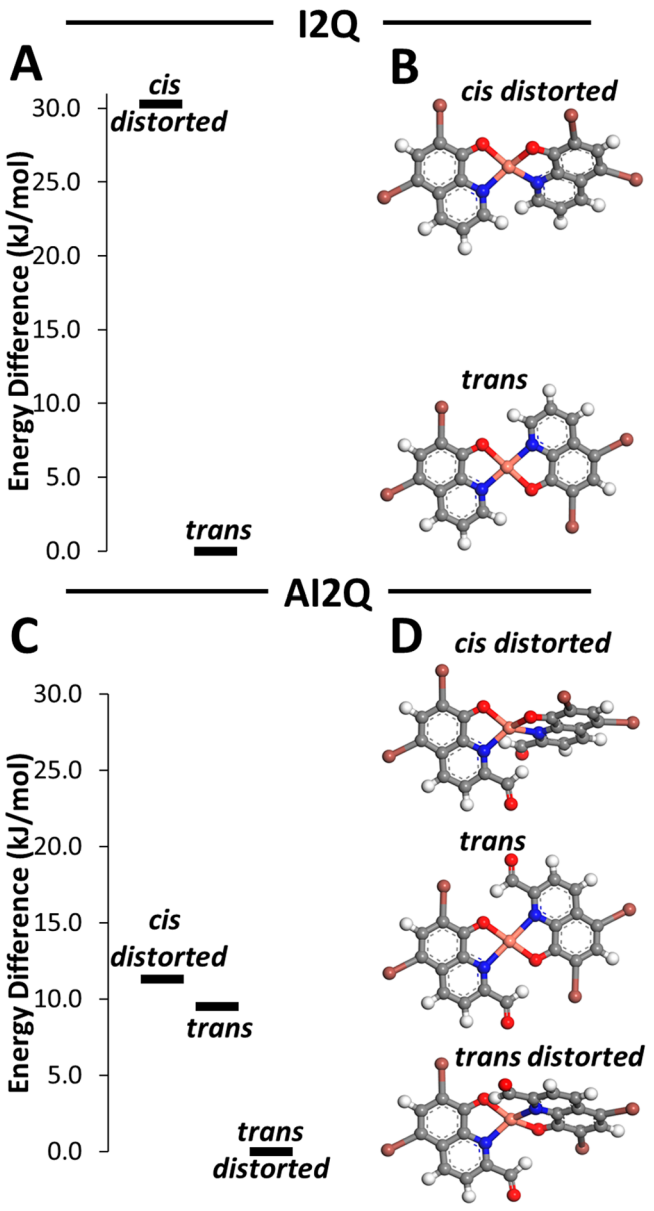

Figure 2. DFT geometry optimized structures of Cu(II) complexes of I2Q and AI2Q. (A) The energy difference between the *cis* distorted and *trans* orientations of the I2Q ligands around the Cu(II) and (B) the geometry optimized structures of the *cis* distorted and *trans* Cu(II)-bis-I2Q complexes. Similarly, (C) shows the energy difference between *cis*, *trans*, and distorted *trans* configurations for the AI2Q ligands around the Cu(II) center. (D) shows the geometry optimized structures for the three configurations of the Cu(II)-bis-AI2Q complex. A conventional color scheme was chosen for each element, such that hydrogen is white, carbon is gray, nitrogen is blue, oxygen is red, copper is pink, and iodine is shown in brown.

95.9° angles of the planar C_{2h} complexes and the 90.0° angles expected for square planar geometry (Table 1). These distorted complexes may be described as approaching a more tetrahedral-like geometry (i.e., expected bond angles of 109.5°), with angle *y* at 102.1−103.2° for most 2-CH_3 substituted 8HQs and an angle *y* of 109.1° for the Cu(II) complex with AI2Q (Table 1). The τ^4 and $\tau^{4\prime}$ parameter values[60,61] of these complexes range from 0.36 to 0.54, where 0 is representative of square planar and 1 is representative of

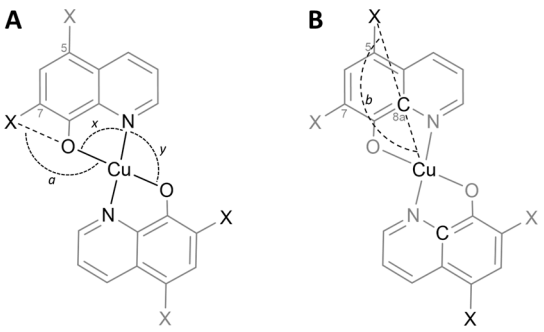

Figure 3. Diagram of angles for Cu(II) 8HQ complexes listed in Table 1, where X = Cl, Br, or I, depending on the 8HQ, as defined in Figure 1. Panel A indicates bond angles *x* and *y* in a Cu(II)-bis-8HQ complex. Angles *a* (panel A) and *b* (panel B) highlight multiple scattering paths that approach linearity.

tetrahedral geometry, suggesting that these 4-coordinate complexes are significantly distorted.

For the most energetically favorable distorted *trans*-Cu(II)-bis-AI2Q complex, electron density from the aromatic ring system is pushed toward the aldehyde substituent in the 2-position (Figure S3D). This redistribution of electron density to the aldehyde groups in the Cu(II)-bis-AI2Q and -AC2Q complexes likely partially explains the decrease in overall energy of the distorted *trans*-Cu(II)-bis complexes. The distortion of the *trans*-Cu(II)-bis-AI2Q and -AC2Q complexes is likely also partially due to steric effects. All the 2-methylated 8HQs studied herein appear to favor a distorted *trans* structure, even though little to no electron density is relocated to the methyl substituents. It therefore seems likely that the 2-CH_3 has a predominantly steric effect, but the 2-CHO appears to have both steric and electronic effects. It was generally observed that in complexes without substituents in the 2-position (e.g., Cu(II)-bis-CQ), distorted *trans* structures always optimized to be planar. Conversely, energy minimized *cis* configuration structures were always distorted.

2.2. Near Edge X-ray Absorption Spectroscopy and High-Energy Resolution Fluorescence-Detected XAS.

XAS near-edge analysis is sensitive to the oxidation state of the metal ion of interest; however, Cu(II) is easily photoreduced in the X-ray beam if the appropriate precautions are not taken to circumvent this common pitfall.[62] In this study, the sample was physically translated after each scan, such that a fresh sample area was illuminated for each energy scan. Additionally, near-edges of consecutive scans from the same sample were examined for changes indicative of Cu(II) → Cu(I) photoreduction, primarily including the loss of the Cu(II) 1s → 3d pre-edge transition and the appearance of the Cu(I) 1s → 4p transition. Despite these precautions some photoreduction inevitably occurs over the course of the 40 min scan, such that the end of the EXAFS region may be partially photoreduced as we have previously shown in metalloproteins.[63]

HERFD-XAS[64] measures X-ray fluorescence with better resolution than the natural line width. In conventional K-edge XAS, the short lifetime of the 1s core hole causes broadening of the spectra with consequent loss of detail and chemical sensitivity. Our Cu K-edge HERFD-XAS utilizes the Cu Kα_1 fluorescence line and effectively observes a small subset of the $2p_{3/2}$ → 1s transitions that give rise to the Cu Kα_1 fluorescence, thus eliminating most of the lifetime broadening from the short 1s core hole lifetime and thereby improving spectral resolution.

https://dx.doi.org/10.1021/acs.inorgchem.0c01356
Inorg. Chem. XXXX, XXX, XXX−XXX

Table 1. Calculated Angles from Geometry Optimized Cu(II) 8HQ Complexes[a]

8HQ	O−Cu−O angle	N−Cu−N angle	O−Cu−N angle[b]	O−Cu−N′ angle[c]	Cu−O···X angle[d]	Cu···C···X angle[e]	τ^4 parameter[f]	$\tau^{4\prime}$ parameter[g]	2-substitution
				8HQs					
8HQ	180.00	180.00	84.19	95.81	N/A[h]	N/A[h]	0.00	0.00	−H
M8Q	150.82	154.12	84.29	102.26	N/A[h]	N/A[h]	0.39	0.38	$-CH_3$
				5-chloro-7-iodo-8HQs					
CQ	180.00	180.00	84.46	95.54	179.73	177.01	0.00	0.00	−H
MCQ	151.06	155.23	83.97	102.26	176.13	175.25	0.38	0.37	$-CH_3$
				5,7-diiodo-8HQs					
I2Q	180.00	180.00	84.23	95.77	179.90	177.92	0.00	0.00	−H
MI2Q	149.55	155.05	83.38	103.23	174.95	175.60	0.39	0.38	$-CH_3$
AI2Q	145.13	138.15	83.49	109.11	177.05	175.56	0.54	0.52	−CHO
				5,7-dichloro-8HQs					
Cl2Q	180.00	180.00	84.13	95.87	174.36	176.92	0.00	0.00	−H
MC2Q	150.34	156.53	83.94	102.09	175.99	175.10	0.38	0.36	$-CH_3$
AC2Q	148.70	153.81	83.44	103.68	175.99	174.96	0.41	0.39	−CHO
				5,7-dibromo-8HQ					
B2Q	180.00	180.00	84.10	95.90	177.23	177.41	0.00	0.00	−H

[a]All angles in degrees. [b]Angle *x* depicted in Figure 3 A. [c]Angle *y* depicted in Figure 3 A. [d]Depicted angle *a* in Figure 3 A. [e]Depicted angle *b* in Figure 3 B. [f]As described by Yang et al.[60] [g]As described by Okuniewski et al.[61] [h]8HQ and M8Q do not have 5- or 7-position halogens.

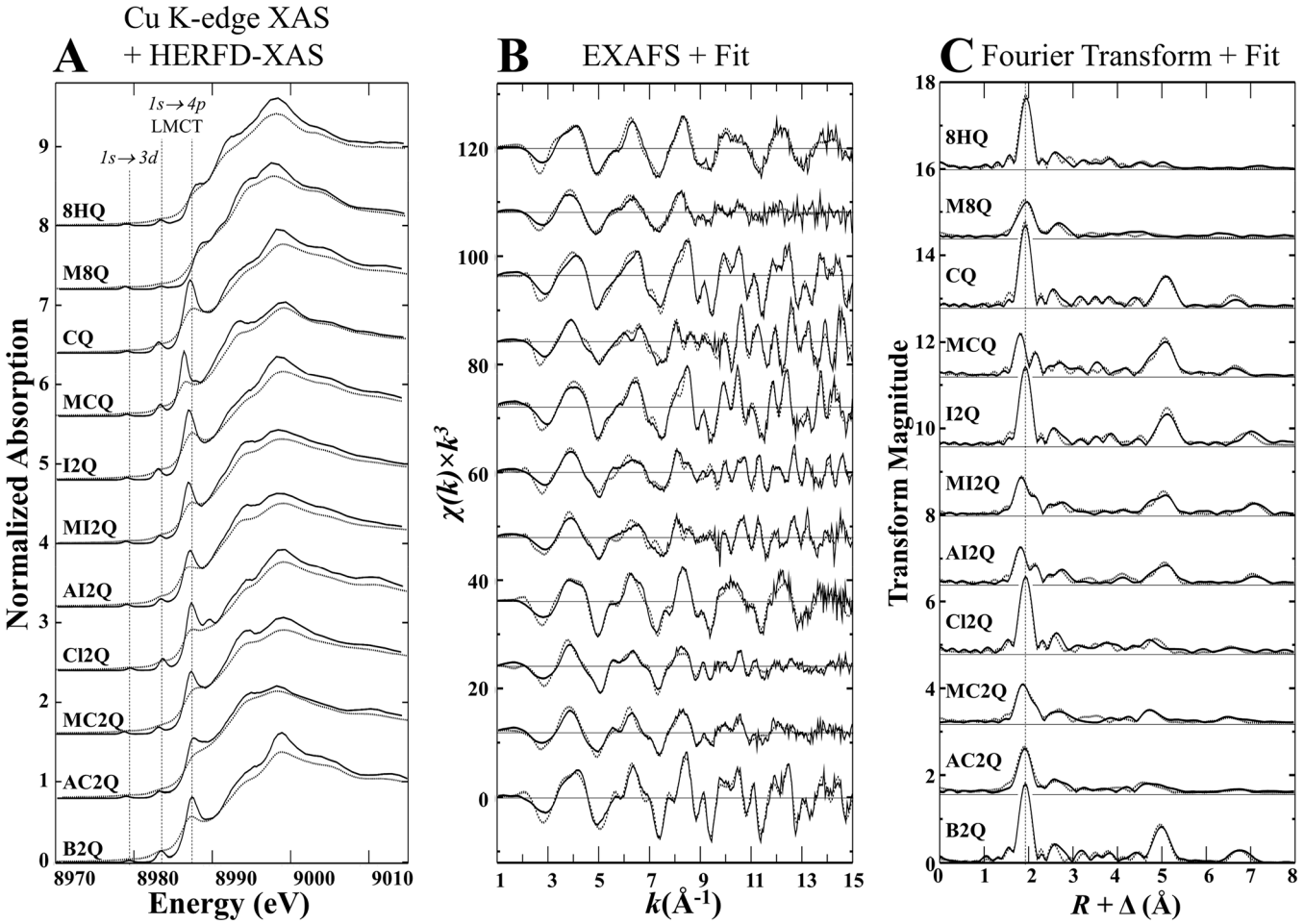

Figure 4. Cu K-edge XAS of Cu(II) complexes with 8HQ and its derivatives. (A) Experimental Cu(II) near-edge spectra from XAS (dashed) and HERFD-XAS (solid line) of 8HQ and studied derivatives. The dashed vertical lines indicate near-edge transitions. A spline was fit to the near-edge spectra, and the spline was normalized to 1; spectra are offset vertically by 0.8 for clarity. Corresponding extended X-ray absorption fine structure (EXAFS) spectra and Fourier transforms from conventional XAS are shown in (B) and (C), respectively. Experimental EXAFS and Fourier transform data are shown in solid black lines; calculated EXAFS and Fourier transform fits are shown as dashed lines. Spectra are also offset vertically for clarity. Horizontal gray lines mark 0 for each individual spectrum. EXAFS spectra are offset by 12 and Fourier transform spectra are offset by 1.6 vertically. Fourier transforms are phase-corrected for Cu−O backscattering.

https://dx.doi.org/10.1021/acs.inorgchem.0c01356
Inorg. Chem. XXXX, XXX, XXX−XXX

Comparisons of XAS and HERFD-XAS experimental near-edge spectra of Cu(II)-bound 8HQs in aqueous surfactant solutions are shown in Figure 4 A. All spectra show a small 1s → 3d transition at approximately 8979 eV, indicative of Cu(II) species. There is also a small peak at approximately 8983 eV, which is well-resolved only in the HERFD spectra (Figure 4 A). Because of the higher photon flux density in a HERFD experiment, samples are more prone to photoreduction than with our conventional XAS; however, this effect is partly offset by the relatively rapid scan rates used for HERFD (∼1−2 min.). Therefore, while the ∼8983 eV feature may arise from photoreduced species, we consider this unlikely because no changes in this near-edge region were observed after prolonged beam exposure without sample translation on a conventional XAS beamline (Figure S4). Assuming that this feature is a true Cu(II) feature, its relatively low energy argues for an assignment as a 1s → $4p_z$ + ligand-to-metal charge transfer (LMCT) shake-down transition, similar to the 8987 eV peak, which will be discussed below. This peak remained unobserved in other experiments because it is not well resolved in conventional XAS experiments. LMCT shake-down transitions are one-photon two-electron events that arise when metal orbitals shift to lower energies following the effective increase in nuclear charge due to 1s photoexcitation in K edge experiments. Therefore, after 1s photoexcitation the metal orbitals lie at lower energies than the ligand orbitals, resulting in consequent LMCT, concomitant with the 1s → 4p excitation. These transitions thus lie below the main 1s → 4p transition and inform of the overlap of ligand and metal 3d orbitals. Because the $4p_z$ orbitals lie at lower energies than the $4p_{xy}$ orbitals in a square planar type geometry as a result of the equatorial ligand field, we therefore tentatively assign this feature as a 1s → $4p_z$ + LMCT shake-down transition (Figure 4 A). The more prominent peak at about 8987 eV also lies at lower energy than the main 1s → 4p peak, and this is tentatively assigned as a 1s → $4p_{xy}$ + LMCT shake-down transition (Figure 4 A). This assignment is supported by preliminary TD-DFT calculations, i.e., where transitions involving the $4p_z$ orbital are predicted to be 4−5 eV lower in energy than those involving the $4p_{xy}$ orbitals. Also in line with this assignment, the 1s → $4p_{xy}$ transition might be expected to have increased intensity relative to the 1s → $4p_z$ transition because both $4p_x$ and $4p_y$ orbitals are involved. Such LMCT shake-down transitions are often thought to be indicative of tetragonal or square planar type Cu(II) coordination geometry, because the ligand field splitting of the 4p manifold is larger in these cases and gives rise to lower energy peak positions.[55,65,66]

In the series of 8HQ Cu(II) complexes shown in Figure 4 A the 1s → 4p + LMCT shake-down transitions are most prominent in aqueous Cu(II) solution complexes of CQ, I2Q, and B2Q, as well as MI2Q and MCQ. Complexes showing intense 1s → 4p + LMCT shake-down transitions are those that are hypothesized to be planar, likely with pseudo square planar Cu(II) coordination, similar to that previously described for Cu(II)-bis-CQ.[55] Interestingly, the near-edge of Cu(II)-bound 8HQ and M8Q, which lack halogen substituents, also lack distinctive 1s → 4p + LMCT shake-down transitions (Figure 4 A). From previous studies and from our DFT calculations Cu(II)-bis-8HQ is expected to be a highly symmetric, coplanar complex with C_{2h} symmetry and would therefore be expected to have pronounced 1s → 4p + LMCT shake-down transitions, if the transition is maximal for complexes closely approaching square planar geometry (i.e., bond angles approaching 90°). While it is possible that the Cu(II)-bis-8HQ complex is not planar, and some crystal structures of this complex suggest slight deviations from the expected coplanar complex in which both 8HQ ligands and the Cu(II) are not all coplanar,[57,58,67−72] it seems plausible that the 1s → 4p + LMCT shake-down transitions could be affected by halogen substitution. The 1s → $4p_{xy}$ + LMCT shake-down transition appears to follow a trend in 5,7-halogenated 8HQ Cu(II) complexes such that peak intensity decreases as follows: Cl & I > I > Cl > Br. In addition, the peak intensity appears to decrease in 8HQ derivatives with the same 5,7-halogen substituents as coplanarity of the complexes decreases, such that 2-H > 2-CH_3 > 2-CHO (Table S3). Therefore, the 1s → 4p + LMCT shake-down transition peak intensity appears to depend both on the coplanarity of the complex (modified by 2-substitution), and on halogen substitution in the 5- and 7-positions. Halogen substituents in the 5- and 7-positions may donate electron density to the 8HQ moiety and help stabilize a more closely square planar geometry, thereby resulting in increased intensity of the 1s → 4p + LMCT shake-down transition peak in the near-edge.

2.3. Extended X-ray Absorption Fine Structure (EXAFS). The EXAFS results of Cu(II)-bound 8HQs in aqueous surfactant solutions are shown in Figure 4 B. The EXAFS oscillations of all Cu(II)-bound 8HQ samples have a similar frequency up to $k \approx 8$, at which point high frequency oscillations attributable to the distant, high atomic number halogen substituents become apparent for Cu(II)-8HQ complexes of CQ, MC2Q, I2Q, MI2Q, AI2Q, MCQ, and B2Q (Figure 4 B). The EXAFS amplitude in this higher k region is greatest for Cu(II) complexes with higher atomic number halogen substituents in the 5- and 7-position, but with no 2-position substitution, such as B2Q, CQ, and I2Q. EXAFS spectra of other Cu(II) complexes have a significant but lower amplitude structure at $k \gtrsim 9$ (e.g., MCQ, MI2Q, and AI2Q). These Cu(II) complexes have large halogen substituents in the 5- and 7-position and also have 2-position substituents. Cu(II) complexes with 5,7-dichlorinated 8HQs, namely, Cl2Q, MC2Q, and AC2Q, appear to lack the high-amplitude, high-k structure observed with other 8HQs. This lack of structure is likely in part because chlorine substituents are weaker backscatterers than bromine or iodine. We note that 8HQ and M8Q lack this high-k structure because they do not have any halogen substituents.

Similar trends are illustrated by the corresponding Fourier transforms (Figure 4 C). The primary backscattering peak in the Fourier transforms of Cu(II)-bound 8HQs without substituents in the 2-position (i.e., 8HQ, CQ, I2Q, Cl2Q, and B2Q) is at 1.926−1.934 Å and arises from first shell interactions with O and N ligands. For most of the 8HQs with substituents in the 2-position (i.e., MCQ, MI2Q, AI2Q, and AC2Q) the primary backscattering peak is slightly shorter, at 1.877−1.903 Å. In some cases (e.g., MCQ, MI2Q, AI2Q, and MC2Q), the primary backscattering peak at ∼1.89 Å has a shoulder or another peak at 2.015−2.064 Å, which suggests distinguishably different ligand bond lengths (Figure 4).

In many Cu(II) 8HQ complexes, there is an intense peak in the Fourier transform at 4.870−5.163 Å, which corresponds to the halogen in the 7-position (e.g., I for CQ), and a peak at 6.636−7.075 Å, corresponding to the halogen in the 5-position (e.g., Cl for CQ). It is unusual to detect backscattering atoms this distant from the absorbing atom (i.e., Cu) in solution

https://dx.doi.org/10.1021/acs.inorgchem.0c01356
Inorg. Chem. XXXX, XXX, XXX−XXX

Table 2. Comparison of Select EXAFS Fit Distances *R* between Cu(II) 8HQ Complexes[a]

	Cu−O	Cu−N	Cu···C	Cu···O	Cu−O···X	Cu···C···X
8HQ	1.929(2)	1.953				
M8Q	1.900(3)	2.021(4)	3.404(7)			
CQ	1.928(1)	1.947			5.141(2)	6.636(5)
MCQ	1.877(3)	2.057(4)	3.595(9)		5.092(2)	6.665(12)
I2Q	1.934(2)	1.951			5.163(2)	6.982(5)
MI2Q	1.893(3)	2.052(4)	3.471(8)		5.067(2)	7.065(4)
AI2Q	1.884(3)	2.064(5)	3.390(10)	4.513(12)	5.088(4)	7.075(7)
Cl2Q	1.931(2)	1.957			4.935(6)	6.662(12)
MC2Q	1.893(3)	2.038(4)	3.409(8)		4.870(5)	6.680(10)
AC2Q	1.903(3)	2.015(6)	3.426(11)	4.649(9)	4.888(10)	6.986(21)
B2Q	1.926(2)	1.953			5.033(2)	6.817(6)

[a]Full fit parameters are detailed in Table S4. Corresponding best-fit plots are shown in Figure 4. The values in parentheses are the estimated standard deviations (esd.) and correspond to the error on the last digit. Although the calculated esd is typically approximately ±0.005, including errors such as imperfect background subtraction, phase-shift calculations, and noise in the data, the actual error is generally accepted to be closer to ±0.01 Å. Values without esd were refined as a set of parameters linked by constant proportion to those of the Cu−O/N paths, and the esd will correspond to that of Cu−O/N.

complexes. These distant substituents are detected in this system because (i) these halogen substituents are heavy, high Z atoms with large backscattering amplitude, (ii) the halogens are connected to the Cu(II) absorber via a relatively rigid ring system, which minimizes the possible disorder in the Cu···X distances, and (iii) multiple scattering involving intervening atoms in the planar 8HQ molecule enhances the amplitude when paths approach colinearity. The arrangement of the atoms in the 8HQ molecule when bound to Cu(II) is unusual in that atoms coincidentally approach a collinear arrangement which gives rise to maximal multiple scattering. Hence, for the 7-position iodine in the Cu(II)-bis-I2Q complex, the Cu(II)−O···I angle at the intervening oxygen is 179.90° (Table 1; Figure 3). Likewise, for the 5-position iodine in the same complex, the angle subtended by fusion carbon atom 8a, angle Cu(II)···C_{8a}···I, is only marginally smaller at 177.92° (Table 1; Figure 3).

The EXAFS amplitude at $k \gtrsim 9$ is largest for Cu(II) complexes with 5,7-dihalogenated 8HQ derivatives and without 2-position substitution (i.e., B2Q, CQ, I2Q), which suggests that the Cu(II)−O···X multiple scattering path (where X= Br, or I) approaches a linear angle of 180°. Planar complexes with C_{2h} symmetry, such as those predicted by DFT (Figure 2), would result in constructive interference from large backscatterers at the same distance (e.g., I). However, Cu(II) complexes with 5,7-dichlorinated 8HQs (i.e., Cl2Q and derivatives) appear to lack this high amplitude, high *k* structure observed with other 5,7-dihalogenated-8HQs. This lack of structure is likely partially because chlorine substituents are weaker backscatterers than Br or I and partly because the C−Cl bond is shorter than that of C−I or C−Br, resulting in a deviation from colinearity and therefore from the maximal multiple scattering amplitude observed for the essentially linear Cu(II)−O···I path (Figure 3; Table 1). However, this lack of structure could also be because the Cu(II) and both 8HQ ligands are no longer all coplanar; for example, the Cu(II) may be out of the plane defined by the 8HQ moieties as is discussed below. Interestingly, an increase in EXAFS frequency and a decrease in EXAFS amplitude is observed with 2-position substitution of Cl2Q (i.e., to form MC2Q or AC2Q). From geometry optimization calculations, it appears likely that the Cu(II)−O···Cl is coincidentally brought closer to a linear path in MC2Q and AC2Q than in Cl2Q in solution (Table 1; Figure 3).

In 2-position substituted complexes that have significant structure at $k \gtrsim 9$ but have a lower EXAFS amplitude (i.e., MCQ, MI2Q, and AI2Q), the angle of the Cu(II)−O···I multiple scattering path again likely deviates from 180°. Distortion from a pseudo square planar geometry that alters the angle of the Cu(II)−O···I path, such that it is farther from the expected maximal backscattering angle of 180°, will dampen the resultant EXAFS amplitude and will reduce the high-frequency EXAFS oscillations due to cancellation of waves that are out of phase (Figure S5; Figure S6).

Intense peaks in the Fourier transform, corresponding to longer range halogens, provide evidence for highly symmetrical structures in which the outer halogens occupy equivalent positions and in which there is substantial multiple scattering due to the intervening oxygen or carbon atom forming close to linear 180° paths (Figure 3; Table 1). In the Fourier transform of some Cu(II) 8HQ complexes (i.e., MCQ, MI2Q, AI2Q, MC2Q, and AC2Q), these longer range peaks appear at two different distances (Figure 4; Table S.4). Double peaks for halogen backscattering at this distance provide further support for distorted bis complexes in which the Cu(II)−O···X path (where X= Cl or I) deviates significantly from 180°. Deviation from 180° results in different distances for the three possible multiple scattering paths through Cu(II)−O···X and results in a splitting of the 7-position halogen peak (∼5 Å peak) in the Fourier transform (Figure S.5; Figure S.7).

One possibility that may account for the observed differences in the EXAFS and Fourier transforms of 2-CH_3 or 2-CHO substituted 8HQs compared with 2-H substituted 8HQs is an in-plane rotation of the 8HQ ligands, such that the Cu(II)−N bond is lengthened and the Cu(II)−O bond remains the same, resulting in the Cu(II)−O···X angle deviating more so from linearity (Figure S.5). As a result of this increasing rotation around the O atom, the primary backscattering peak splits into two resolved peaks corresponding to the Cu(II)−O and Cu(II)−N bond distances. The 5 Å peak corresponding to the Cu−O···X distance is also split into 2 poorly resolved peaks as the Cu(II)−O···X angle deviates increasingly from linearity, and the ∼7 Å peak corresponding to the Cu(II)···X distance to the 5-position halogen increases

https://dx.doi.org/10.1021/acs.inorgchem.0c01356
Inorg. Chem. XXXX, XXX, XXX−XXX

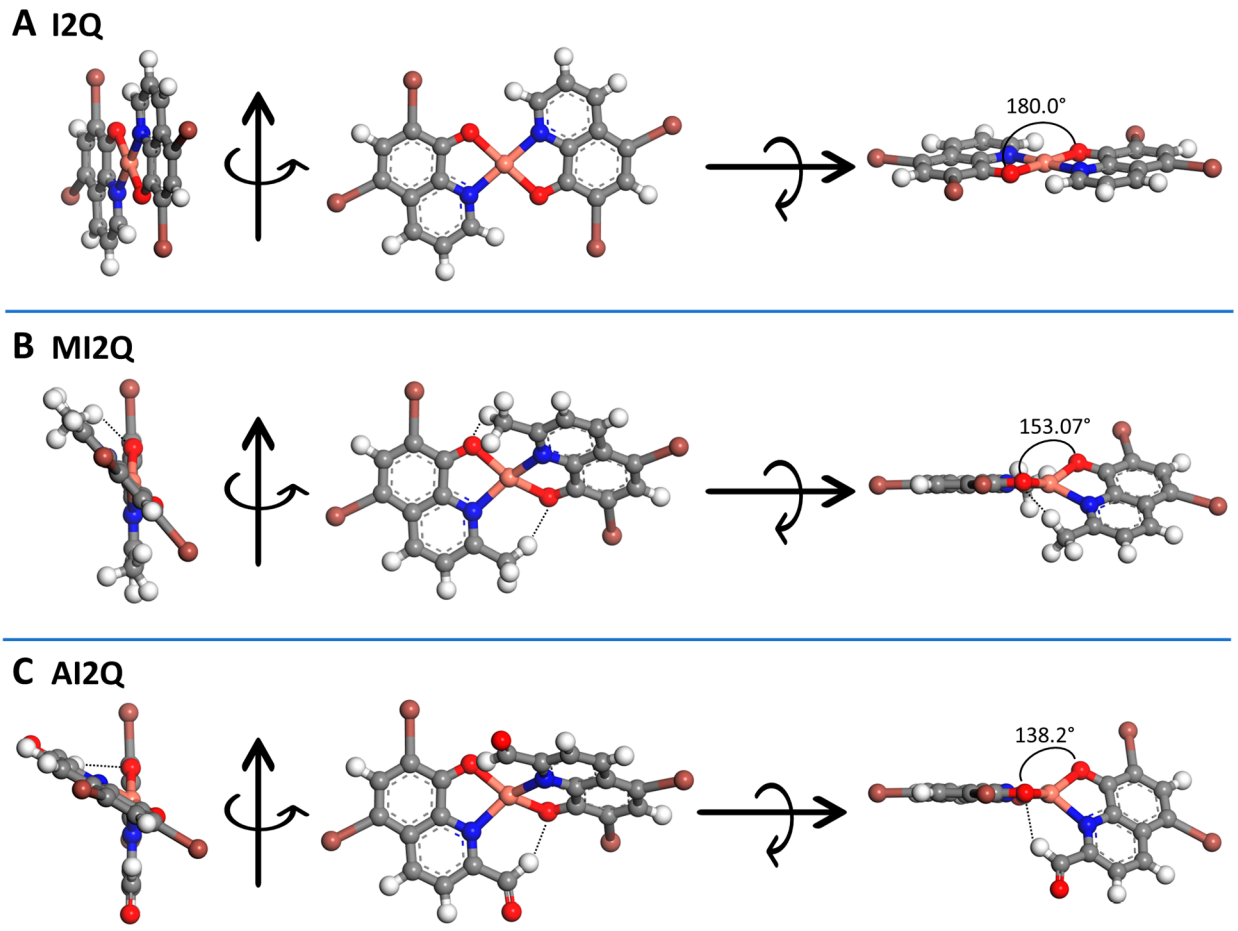

Figure 5. DFT geometry optimized Cu(II)-bis-8HQ structures, highlighting the degree of out-of-plane rotation for 2-substituted 8HQ derivatives. The planar Cu(II)-bis-I2Q structure is shown in (A), the distorted Cu(II)-bis-MI2Q structure is shown in (B), and the highly distorted Cu(II)-bis-AI2Q structure is shown in (C). A typical color scheme was chosen for each element, such that hydrogen is white, carbon is gray, nitrogen is blue, oxygen is red, copper is pink, and iodine is shown in brown. Hydrogen bonding interactions are shown as dashed lines from the methyl proton of one MI2Q to the phenol oxygen of the other MI2Q (B) and from the aldehyde proton of one AI2Q to the phenol oxygen of the other AI2Q (C).

(Figure S5). The ~7 Å peak is also dampened slightly as the angle deviates further from 180°.

Another possibility is that the Cu(II) atom may no longer be coplanar with the 8HQ molecules, which would also result in a smaller Cu(II)−O···X angle (Figure S6). As a result of this hypothetical rotation of the Cu(II) out of the ligand plane, the 5 Å peak corresponding to the Cu(II)−O···X distance decreases in both intensity and distance as the Cu(II)−O···X angle deviates further from linearity. Likewise, the Cu(II)···X distance to the 5-position halogen (7 Å peak) becomes shorter and also decreases in intensity as the Cu(II)···C_{8a}···X angle deviates further from linearity. However, the Cu(II)−O and Cu(II)−N distances remain unchanged and appear in the Fourier transform as a single primary backscattering peak (Figure S6). Additionally, the two 8HQ molecules may remain equivalent to each other but may not be coplanar (Figures 2 and S3). It is likely that a combination of these above-mentioned rotations may result in the structure(s) that best fit the EXAFS data.

2.4. Geometry Optimization and Curve-Fitting of the EXAFS. Scattering paths for geometry optimized structures of Cu(II)-bound 8HQ complexes were calculated using FEFF (ver. 8.25) and were used in the curve-fitting program, OPT, in the EXAFSPAK suite of XAS analysis programs[73] to determine the best fit model for the EXAFS spectra. Possible structures for Cu(II)-8HQs were fit to the Cu K-edge EXAFS; curve-fitting results for Cu(II)-bis-8HQs are shown in Figure 4, summarized in Table 2, and described in full in Table S4. The best fit structure for XAS spectra of the Cu(II)-bis-CQ complex in DMSO has been published previously,[55] and a highly similar structure is found to be the best fit for Cu(II)-bis-CQ in aqueous solution here. Best-fit structures of Cu(II)-bis-8HQ, -B2Q, -I2Q, and -Cl2Q similarly contain Cu(II) coordinated through the phenolate oxygen and nitrogen ligands in a pseudo square planar geometry (Figure 4 A). Best-fit structures for 8HQs with 2-CH_3 substituents, Cu(II)-bis-MC2Q, -MI2Q, -MCQ, and -M8Q, also show Cu(II) coordination through oxygen and nitrogen ligands; however, the quinolin-8-olate anions are rotated such that one 8HQ ligand is approximately 30° out of the plane defined by the other 8HQ ligand, and such that the expected pseudo square planar geometry is distorted to the extent that some of the bond angles approach a more tetrahedral-like geometry (Figure 5 B; Table 1). Best-fit structures for 2-aldehyde-substituted Cu(II)-bis-AC2Q and -AI2Q also have a 4-coordinate Cu(II) center with oxygen and nitrogen ligands; however, the 2-CHO results in the rotation of the 8HQ molecules such that one 8HQ is at approximately 40° from the plane defined by the other 8HQ ligand (Figure 5 C). This greater deviation from planarity could be due to the more

https://dx.doi.org/10.1021/acs.inorgchem.0c01356
Inorg. Chem. XXXX, XXX, XXX−XXX

Table 3. Summary of EPR Parameters for Cu(II)-8HQ and Cu(II)-M8Q Complexes under Various Solution Conditions at 77 K

complex	solvent conditions	$g_{\parallel}$	$g_{\perp}$ $g_x g_y$	$A_{\parallel}$ (mHz)	$A_{\perp}$ (mHz) $A_x A_y$	ref
Cu(II) 8HQ[a]	60% chloroform 40% toluene	2.172	2.042	486	75	Gersmann and Swalen (1962)[87]
Cu(II)-bis-8HQ[b]	50% chloroform 50% toluene	2.202	2.052	537		Yordanov et al. (1975)[90]
Cu(II)-bis-8HQ[b]	50% chloroform 50% toluene	2.205	2.052	564		Yordanov and Alexiev (1983)[94]
Cu(II)-bis-8HQ[b]	neat dimethylformamide	2.244	2.075	501	75	Anjaneyulu et al. (1986)[56]
Cu(II)-bis-8HQ[c]	60% chloroform 40% toluene	2.219	2.046	529	68	Cozar et al. (2010)[89]
Cu(II)-bis-8HQ[c]	70% carbon tetrachloride 30% ethanol	2.221	2.042	527	70	Cozar et al. (2010)[89]
Cu(II)-bis-8HQ[c]	75% chloroform 25% ethanol	2.224	2.049	517	62	Cozar et al. (2010)[89]
Cu(II)-bis-8HQ[c]	60% pyridine 40% chloroform	2.231	2.051	505	64	Cozar et al. (2010)[89]
^{63}Cu(II)-bis-8HQ[b]	80% methanol 20% water	2.247		555		Sgarlata et al. (2018)[48]
^{63}Cu(II)-bis-8HQ	**DTAB/MOPS, pH 7.4**	**2.202**	**2.051/2.036**	**620**	**114/74**	**this work**
^{63}Cu(II)-bis-M8Q	**DTAB/MOPS, pH 7.4**	**2.230**	**2.066/2.030**	**477**	**22/40**	**this work**

[a]Concentration or ratio of Cu(II) and 8HQ not reported. [b]Concentration of Cu(II) and 8HQ not reported. [c]8HQ concentration reported to be 7 mg/mL.

electron-withdrawing nature of the aldehyde group or because of steric effects from the bulkier substituent. Not surprisingly, individual 8HQ ligands, including all atoms except the methyl protons, were always calculated to be very close to planar regardless of the extent to which the copper complex deviates from the pseudo square planar geometry.

Overall, our data suggest that, in solution, 5,7-dihalogenated 8HQs without substituents in the 2-position are planar bis-Cu(II)-complexes that coordinate Cu(II) in a 2 ligand/1 metal ratio, resulting in a pseudo square planar geometry (i.e., planar, with N−Cu−O bond angles approaching 90°; Table 1). This proposed structure is highly similar to that previously published for CQ[55] and is in agreement with crystal structures of various Cu(II)-bis-complexes of 8HQs lacking 2-position substituents (e.g., CSDS entries CIFFED,[74] CUHQCB,[75] VERBUQ,[76] XAGKIZ,[77] DOBMAK,[34] NABMEJ,[53] QESMIL,[78] and QIYQUL.[79]). 8HQs with substituents in the 2-position show altered Cu(II) coordination environments, likely because the 8HQ ligands and the Cu(II) are not all coplanar; although less likely, it could also be because the substituents preclude the formation of Cu(II)-bis-complexes through steric or other effects. Distortion of the planar bis complexes observed with 2-position substitution appears to agree with crystallographically determined structures of various 2-substituted 8HQ derivatives that also show 4-coordinate Cu(II) coordination distorted from the pseudo square planar-like geometry of 2-H 8HQs (e.g., CSDS entries KAFTOA,[80] KAFTUG,[80] QAFNOD,[81] QAFWIG,[81] QUJTAR,[82] and YIGROW[83]). However, not all crystal structures of 2-position-substituted 8HQ complexes with Cu(II) show a significantly distorted 4-coordinate geometry. For example, some 2-position-substituted 8HQs result in coplanar complexes with Cu(II) in which both 8HQ ligands and the Cu(II) are coplanar but the bulky substituents (e.g., a 2,2-bis-(ethoxycarbonyl)ethyl group, CSDS entry GECYAP;[84] or a 2-(2,6-dichlorophenyl)vinyl group, CSD entry FINBAH[85]) are not. There is a strong energetic preference for Cu(II) to approach square planar geometry, including similar Cu(II)−O and Cu(II)−N bond lengths and bond angles close to 90°, unless this cannot be achieved because of unfavorable steric interactions from the substituent in the 2-position, such as those we observe herein.

2.5. Electron Paramagnetic Resonance Spectroscopy.

EPR of Cu(II) complexes can provide information about the symmetry and bonding environment around the Cu(II) center. EPR has been used extensively to study the Cu(II) 8HQ complex.[56,86−89] Early EPR studies of polycrystalline Cu(II)-bis-8HQ reported g-values characteristic of axial symmetry and 2N2O coordination in *trans* around the Cu(II) center ($g_{\parallel}$ = 2.287, $g_{\perp}$ = 2.066).[86] Bonding parameters α^2 (measure of the σ-bonding to the four ligands in the plane), β^2 (measure of the in-plane π-bonding), and γ^2 (measure of the out-of-plane π-bonding) were also calculated to be 0.820, 0.840, and 1, respectively, suggesting that bonding of the Cu(II) to the ligands is covalent and in-plane.[86] Interestingly, several EPR studies of the Cu(II) 8HQ complex in solution have provided different results dependent on solvent conditions, which also differ slightly from those found with the crystalline complex (Table 3).[86,87,89,90]

Further EPR studies of Cu(II) complexes of 8HQ, Cl2Q, B2Q, and I2Q in powdered form have been published.[56] In these studies, Anjaneyulu et al.[56,88] used the effective field per unpaired electron parameter χ, which primarily depends on the local Cu(II) environment,[91,92] as well as molecular orbital coefficients α^2 and β^2, to describe the Cu(II) complexes of 8HQ, Cl2Q, B2Q, and I2Q. The average χ value for a Cu(II) environment with two oxygen and two nitrogen ligands was reported to be −3.918,[93] and the average was calculated to be −3.920 for Cu(II) complexes of 5,7-dihalogenated 8HQs.[56] The molecular orbital coefficients suggested that in-plane π-bonding is as strong as that of σ-bonding in Cu(II) 8HQ complexes, and halide substitution does not affect π-bonding

https://dx.doi.org/10.1021/acs.inorgchem.0c01356
Inorg. Chem. XXXX, XXX, XXX−XXX

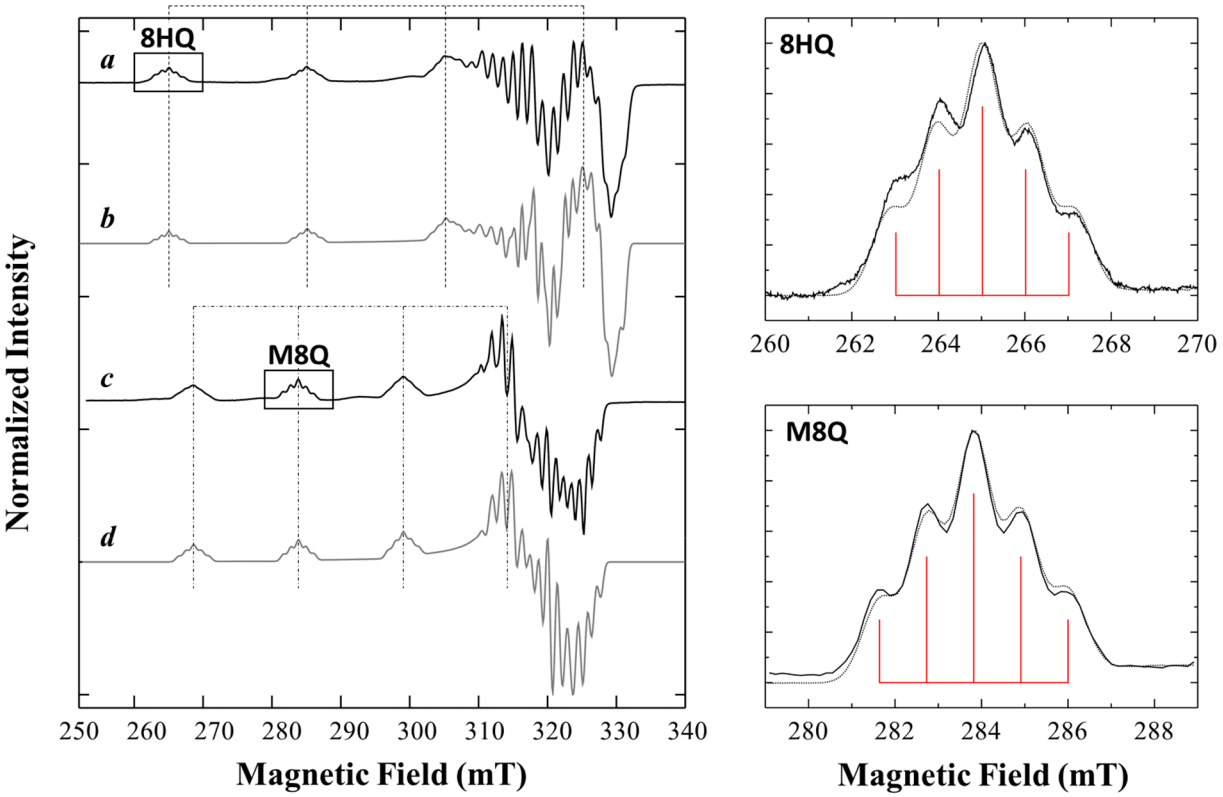

Figure 6. EPR of frozen solutions of Cu(II) 8HQ and M8Q in 400 mM DTAB, 100 mM MOPS at pH 7.4. Spectra are listed as (a) frozen solution spectra of 0.5 mM 8HQ + 0.25 mM $^{63}CuCl_2$, (b) a simulation of (a), (c) frozen solution spectra of 1.25 mM M8Q + 0.25 mM $^{63}CuCl_2$, and (d) simulation of (c). Dashed lines indicate 4-line patterns characteristic of Cu(II) species. Boxes indicate regions expanded in the rightmost panels, in which spectra are shown as solid lines and simulations are shown as dashed lines. Red lines indicate 5-line patterns predicted by ^{14}N hyperfine splittings of 10.9 and 10.0 G in Cu(II)-bis-8HQ and -M8Q, respectively, from 2 equiv of nitrogens. EPR simulation parameters are detailed in Table 3.

character.[56,86,87] There were reportedly no significant differences in either the spin Hamiltonian parameters or in the molecular orbital coefficients of Cu(II)-bound 8HQ, Cl2Q, B2Q, or I2Q.[56] The Cu(II) 8HQ complexes of 8HQ, Cl2Q, and B2Q showed g-values consistent with axial symmetry, while the Cu(II) I2Q complex showed an isotropic g-value.[56]

EPR of the Cu(II) CQ complex has also been previously published.[48,55] Sgarlata et al. determined the g-values of the Cu(II)-bis-CQ complex to be $g_{\|}$ = 2.243 and $g_{\perp}$ = 2.047 in DMF and $g_{\|}$ = 2.242 and $g_{\perp}$ = 2.049 in DMSO. EPR magnetic parameters determined for both Cu(II)-bis-CQ and Cu(II)-bis-8HQ are thought to be indicative of a tetragonally elongated pseudo-octahedral arrangement around the Cu(II), with an equatorial Cu(II)N_2O_2 chromophore.[48] These spectra in DMF appear surprisingly different from spectra in DMSO, which was previously published by our group.[55] These differences are likely to be attributed to either differences in the concentration of Cu(II) and CQ used or the relative ratios of ligand to metal.

In this study, EPR spectra of ^{63}Cu(II)-bis-8HQ and ^{63}Cu-(II)-bis-M8Q in frozen aqueous solutions were examined to further probe the different Cu(II) coordination environments in 2-H and 2-CH_3 substituted 8HQs. To the best of our knowledge, the EPR spectra of Cu(II)-bis-M8Q shown in Figure 6 are the first to be reported on a 2-position methyl-substituted 8HQ Cu(II) complex. EPR spectra of Cu(II)-bis-8HQ were found to resemble spectra previously published for the Cu(II)-bis-CQ complex in DMSO[55] when excess ligand was present and relatively high concentrations of both 8HQ (≥2.5 mM) and Cu(II) (≥0.5 mM) were used (Figure S8). These higher concentration spectra do not appear magnetically dilute and more closely resemble powder EPR spectra of Cu(II)-bis-8HQ complexes in the literature.[56] These magnetically nondilute spectra may be a result of distant π-stacking though the ring system of Cu(II)-bis-8HQ complexes, which would result in Cu(II) atoms separated by approximately 7−10 Å, as has been shown in the unit cell of several crystal structures of Cu(II)-bis-8HQs.[34,57,69,75] We have found little evidence of compact π-stacking based on our EXAFS data (Figure 4). Specifically, we do not see evidence of Cu···Cu scattering, which would be expected to be significant if Cu(II)-bis-8HQ complexes were stacking such that the Cu(II) centers were $\lesssim$7 Å apart. Additionally, we do not see peaks $\gtrsim$5 Å in the Fourier transforms of Cu(II)-bis-8HQ complexes in which there are no 5,7-halides (e.g., see 8HQ or M8Q spectra, Figure 4). Taken together, these results likely suggest that any π-stacking is distant, such that the Cu(II) centers are $\gtrsim$7 and $\lesssim$10 Å apart.

When the complexes were prepared at lower concentrations (i.e., [Cu] = 0.25 mM and [8HQ] ≤ 1.25 mM), EPR spectra were more similar to frozen solvent spectra previously published for Cu(II)-bis-8HQ,[48,90] Cu(II)-bis-B2Q,[56] and the Cu(II)-bis-CQ complex.[48] Spectra of ^{63}Cu(II)-bis-8HQ and -M8Q show a 4-line pattern typical for Cu(II) complexes (Figure 6). Nitrogen hyperfine structure in both the $g_{\|}$ and $g_{\perp}$ regions is significant in spectra of ^{63}Cu(II) complexes of both 8HQ and M8Q. EPR spectra were simulated to generate the g and A values listed in Table 3, and the simulated spectra are

https://dx.doi.org/10.1021/acs.inorgchem.0c01356
Inorg. Chem. XXXX, XXX, XXX−XXX

shown in Figure 6. The spectra of Cu(II) complexes of 8HQ and M8Q were both best simulated by rhombic g values (where $g_x \neq g_y \neq g_z$) and by including splitting-dependent broadening, simulated as A strain.[95] The observation of an anisotropic rhombic g tensor with $g_x \neq g_y$ is expected from the fact that these complexes do not possess true axial symmetry; moreover, the hyperfine coupling is also expected to show rhombic symmetry. Calculated EPR parameters follow similar trends to the experimental spectra, with rhombic g values for both complexes. The calculated EPR parameters for Cu(II)-bis-8HQ predicted g values of 2.049, 2.083, and 2.203 for g_x, g_y, and g_z, respectively, and that for Cu(II)-bis-M8Q predicted g values of 2.045, 2.083, and 2.199 for g_x, g_y, and g_z, respectively.

Regions with well-defined N hyperfine were found to be best simulated by 2 equiv of N-donor ligands, generating a 5-line pattern with intensities in a 1:2:3:2:1 ratio, and with ^{14}N hyperfine splitting of 10.9 G (15.3 MHz) for the ^{63}Cu(II)-bis-8HQ complex and 10.0 G (14.0 MHz) for the ^{63}Cu(II)-bis-M8Q complex. DFT-calculated nitrogen hyperfine couplings follow a similar trend to the experimental spectra, predicting A_z (^{14}N) values of 33.6 MHz for Cu(II)-bis-8HQ and A_z (^{14}N) values of 31.2 MHz for Cu(II)-bis-M8Q. The ^{14}N hyperfine value determined for the ^{63}Cu(II)-bis-8HQ complex is consistent with previously published values.[89,90,94] These findings provide further evidence for Cu(II)-bis-8HQ and -M8Q complexes in which both N-donor atoms are in equivalent positions relative to the Cu(II) center. The slightly larger ^{14}N coupling for Cu(II)-bis-8HQ relative to Cu(II)-bis-M8Q is consistent with the distortion away from planar geometry for the latter complex, and with DMol^3 DFT calculations of the nitrogen spin densities, which give values of 0.09 and 0.07 for the pyridine nitrogens, respectively.

3. CONCLUSIONS

Herein, we have provided a detailed structural investigation of the Cu(II) complexes formed with select 8HQs of interest using synchrotron XAS and HERFD-XAS, as well as EPR and DFT calculations. For many 8HQs, this is the first study to investigate these Cu(II) complexes in aqueous solution, and for some, this is the first structural investigation reported to date. The previous lack of complete information on the solution chemistry of 8HQs, and other similar biologically relevant molecules, has made it difficult to predict their *in vivo* action. Herein, we attempt to connect the *in vitro* structural information with *in vivo* properties desired for effective treatment of diseases of metal ion dyshomeostasis.

3.1. Cu(II) Coordination in CQ and Similar 8HQ Conformers. The solution structure of Cu(II)-bis-CQ in DMSO has been published previously and was found to be planar, with a pseudo square planar type Cu(II) center.[55] Similarly, the 5,7-dihalogenated 8HQ conformers studied here also appear to bind Cu(II) in a square planar-like geometry with two bidentate 8HQ ligands. Specifically, Cu(II)-bis-complexes with 8HQ, B2Q, CQ, I2Q, and Cl2Q are highly planar and even a slight deviation in planarity results in a less stable (higher-energy) structure in DFT-based energy calculations. The HOMO to LUMO transition of these 8HQ derivatives is from a predominantly ligand-based orbital to an orbital with significant contributions from Cu 3d orbitals. The Cu(II) near-edge spectra show a prominent peak at ~8987 eV which is attributable to a 1s → 4p + LMCT shake-down transition and is often described as being indicative of square planar type Cu(II) coordination geometry. Many of these Cu(II)-8HQ complexes show significant structure in the EXAFS region at high k-range, attributable to long distance halogen interactions that are further enhanced by multiple scattering. This structure in the EXAFS spectrum suggests these complexes show coplanarity, with both 8HQ molecules and the Cu(II) all coplanar and with high symmetry. Coplanar, symmetrical Cu(II)-bis-5,7-dihalogenated-8HQ complexes and a fortuitously linear path from the Cu(II) absorber to halogen substituents in the 7-position allow for greater backscattering from these large substituents at the same distance from the primary absorbing atom. Likewise, peaks in the Fourier transform corresponding to longer range halogens provide additional evidence for highly symmetrical, coplanar Cu(II)-bis-5,7-dihalogenated-8HQ structures; multiple scattering at this distance is much more probable if the path is linear and contributions from halogens at the same distance are additive.

3.2. Substituents in the 2-Position of 8HQs Modify Cu(II) Coordination Geometry. Through comparisons of spectra from planar Cu(II)-bis-8HQ derivative complexes with the Cu(II) complexes of 8HQ derivatives with substituents such as $-CH_3$ and $-CHO$ in the 2-position (see Figure 1), it is evident that substituents in this position can alter structural aspects of the Cu(II) 8HQ complex, including planarity and coordination geometry. Specifically, substitution by a methyl group in the 2-position of 8HQ and its derivatives CQ, I2Q, and Cl2Q to form M8Q, MCQ, MI2Q, and MC2Q, respectively, results in a loss of planarity in DFT-based structure calculations (i.e., the Cu(II) and the atoms from both 8HQ moieties are no longer all coplanar). Cu K-edge near-edge spectra show less intense 1s → 4p + LMCT shake-down transitions in the near-edge of 2-position methylated 8HQ Cu(II) complexes, which is consistent with a deviation from coplanarity, compared with related Cu(II) complexes that lack 2-position substituents. The EXAFS amplitude at high k is damped for these complexes, likely because multiple scattering paths to distant halogen backscatterers appear at different distances as a result of nonlinear Cu(II)−O···X paths, and their EXAFS oscillations therefore no longer constructively interfere. It is most evident from the Fourier transforms that halogen backscatterers in these complexes are not arranged linearly with the Cu(II)−O bond because the resultant multiple scattering paths often appear as two overlapping peaks. Methyl substituents in the 2-position result in distortion of planar Cu(II)-bis-8HQ complexes, likely due to steric effects, such that the planes of individual 8HQ molecules are no longer coplanar with each other and the point group symmetry is reduced. The distorted *trans* structures may be viewed as forming a "propeller" arrangement about the metal center, where the 2-position methyl groups are pointed up and the planes are tilted with respect to each other. Hydrogen bonding from the methyl proton of one 2-CH_3 8HQ to the phenol oxygen of the other 2-CH_3 8HQ, at a DMol^3 DFT-computed H···O distance of 2.35 Å, likely helps to stabilize this arrangement.

Interestingly, substitution with an aldehyde in the 2-position of 8HQ derivatives I2Q and MC2Q to form AI2Q and AC2Q, respectively, results in more significantly distorted Cu(II) centers compared with their corresponding 2-CH_3 compounds. The HOMO to LUMO transition of the 2-CHO 8HQ derivative Cu(II) complexes is likewise from a predominantly ligand-based orbital to an orbital with significant contributions from Cu 3d orbitals; however, electron density from the aromatic ring system is pushed toward the aldehyde

https://dx.doi.org/10.1021/acs.inorgchem.0c01356
Inorg. Chem. XXXX, XXX, XXX−XXX

substituent in the 2-position. Similar to the 2-CH_3 8HQ derivatives discussed above, 2-CHO 8HQ derivatives AI2Q and AC2Q also show less intense 1s → 4p + LMCT shake-down transitions in the Cu near-edge, as well as dampened EXAFS amplitude at high k (likely because multiple scattering paths to distant halogen backscatterers are nonlinear), and the resultant paths appear as two overlapping peaks in the EXAFS Fourier transforms. The highly electron-withdrawing oxygen of the aldehyde group likely causes some of the electron density from the π system to be pushed toward the aldehyde oxygen, reducing the strength of the Cu(II)−N bond. The repulsion of these highly electron-dense groups results in a distortion of the typical pseudo square planar coordination around the Cu(II) similar to that observed for 2-CH_3 substituted 8HQ derivatives, but with greater rotation of one 2-CHO substituted 8HQ moiety from the plane defined by the other 2-CHO substituted 8HQ moiety (i.e., up to 40° in Cu(II)-bis-AI2Q). This distortion is most likely due to both steric and electronic effects. Similar to the case with 2-CH_3 8HQs, hydrogen bonds from the aldehyde proton of one 2-CHO 8HQ to the phenol oxygen of the other 2-CHO 8HQ, at a DMol^3 DFT-computed H···O distance of 2.34 Å, likely helps to stabilize this arrangement.

3.3. Implications for Drug Design. In the development of novel 8HQ drug compounds, substituents may be used to tune the properties of the metal-bound complex and potentially improve drug efficacy. Halogen substituents in the 5- and 7-positions may be used to tune the hydrophobicity of an 8HQ complex with Cu(II) and therefore potentially impact membrane permeability and trafficking of this drug complex. Substituents in the 2-position may be used to tune the Cu(II) coordination environment and therefore the planarity, as well as other properties of the resultant drug complex. Because the 8HQ family of drug compounds is used to treat several metal trafficking and storage diseases, which often require compounds to cross the blood−brain barrier, the properties of these compounds and their metal-bound complexes may have a significant impact on their ability to reach the brain and restore metal ion homeostasis.

4. MATERIALS AND METHODS

4.1. Synthesis of 8HQs. Unsubstituted 8-hydroxyquinoline (8HQ; Sigma-Aldrich, USA), 5-chloro-7-iodo-8-hydroxyquinoline (CQ; Sigma-Aldrich, USA), 5,7-dibromo-8-hydroxyquinoline (B2Q; Alfa Aesar, Thermo Fisher Scientific, USA), 5,7-dichloro-8-hydroxyquinoline (Cl2Q; Sigma-Aldrich, USA), 5,7-diiodo-8-hydroxyquinoline (I2Q; Sigma-Aldrich, USA), 8-hydroxy-2-methylquinoline (M8Q; Sigma-Aldrich, USA), and 5,7-dichloro-8-hydroxy-2-methylquinoline (MC2Q; Sigma-Aldrich, USA) were purchased and used as received.

5-Chloro-7-iodo-8-hydroxy-2-methylquinoline (MCQ) was synthesized following published protocols.[96] Briefly, iodine trichloride (10 g, 42.80 mmol) in conc. HCl (80 mL) was added dropwise to a solution of M8Q (6.60 g, 41.5 mmol) in conc. HCl (10 mL) with stirring for 30 min. The resultant yellow solid was filtered, dried, and crystallized from hot ethanol to yield pale green crystals.

5,7-Diiodo-8-hydroxy-2-methylquinoline (MI2Q) was also synthesized following previously published methods.[96] Briefly, iodine monochloride (13.5 mL, 1.0 M) was added dropwise to a solution of M8Q (1.00 g, 6.28 mmol) in conc. HCl (10 mL) with stirring. The reaction was then stirred for 1.5 h. The yellow precipitate was filtered and stirred in water (50 mL) 3 times for 1 h. It was then filtered again and recrystallized from hot ethanol to yield beige needle-like crystals.

5,7-Diiodo-8-hydroxyquinoline-2-carboxaldehyde (AI2Q) synthesis followed previous protocols.[97] *N*-Iodosuccinimide (115 mg, 0.65 mmol) was added to a stirred solution of 8-hydroxyquinoline-2-carbonitrile (50 mg, 0.29 mmol) in 15 mL of toluene at room temperature, and the mixture was stirred for 10 h. Crude material was absorbed onto silica using dichloromethane and concentrated *in vacuo*. Product was purified as a pale-yellow solid by flash column chromatography using methylene chloride.

5,7-Dichloro-8-hydroxyquinoline-2-carboxaldehyde (AC2Q) was synthesized as previously published.[98] Briefly, selenium dioxide (1.66 g, 15 mmol) was added to a solution of MC2Q (1.59 g, 10 mmol) in 1,4-dioxane (20 mL). The reaction mixture was heated to 80 °C and stirred for 12 h. The crude product was filtered and evaporated under reduced pressure to dryness. The residue was purified by silica gel flash column chromatography (ethyl acetate/petroleum ether, 1:20 v/v) as a yellow solid.

4.2. XAS Sample Preparation. Solutions of 400 mM dodecyl trimethylammonium bromide (DTAB) were prepared in 100 mM MOPS, and the pH was adjusted to ∼7.4. Solutions were sonicated for ∼10 min, or until all the DTAB dissolved, in a 60 °C water bath. Stock 8HQ solutions were prepared by dissolving prepared powders in the room temperature surfactant solution to a final concentration of 10 mM and sonicating them for ∼5 min. Aqueous Cu(II) 8HQ samples were prepared by diluting 8HQ stock solutions to a final concentration of 4 mM (2 8HQ: 1 Cu) in 400 mM DTAB buffered with 100 mM MOPS at pH 7.4; Cu(II) was then added from an aqueous stock solution of 100 mM $CuCl_2$ to a final concentration of 2 mM. Solutions were sonicated for ∼5 min or until completely dissolved. Aqueous samples were loaded into 3 mm, metal-free, acrylic sample cuvettes sealed with metal-free tape, flash frozen in isopentane cooled with liquid nitrogen, and stored at 77 K prior to experimentation.

4.3. Synchrotron High-Energy Resolution Fluorescence Detected X-ray Absorption Spectroscopy. Near-edge HERFD-XAS measurements were carried out on BL 6−2 at SSRL with the SPEAR3 storage ring containing 500 mA at 3.0 GeV. Using a similar setup to that previously described,[63] a Si(311) double-crystal monochromator with an energy resolution at the Cu K-edge of ∼0.3 eV was used with a 6-element array of Si(444) crystal analyzers to record the Cu Kα_1 emission line.[99] Harmonic rejection was achieved by setting the cutoff energy of the upstream Rh-coated mirror to 18 keV. Incident and transmitted X-rays were monitored using helium-filled and nitrogen-filled gas ionization chambers, respectively. An in-hutch photon shutter was used to prevent exposure of the sample when data were not actively being recorded. Aluminum filters upstream of the incident ion chamber were used to minimize X-ray exposure and the resulting photodamage. Samples were maintained at 10 K using a liquid helium flow cryostat (Oxford Instruments, Abingdon, U.K.) and were inclined at 45° to the incident X-ray beam to facilitate measurement of X-ray fluorescence, giving an effective incident X-ray path length of 2.8 mm. Energy calibration of the monochromator was determined relative to the lowest-energy inflection of a Cu foil, which was assumed to be 8980.3 eV. Each data set is a collection of 20 scans. To decrease the risk of photoreduction of Cu(II) compounds, samples were scanned at multiple positions on the same sample (i.e., using a 110 × 400 μm beam and 0.3 mm vertical and 1.0 mm horizontal movements) and near-edges of successive scans were compared for loss of the 1s → 3d transition, which is indicative of photoreduction.[62] Data reduction and analyses were carried out as previously described[100] using the EXAFSPAK suite of computer programs.

4.4. Synchrotron X-ray Absorption Spectroscopy. XAS measurements were conducted at the Stanford Synchrotron Radiation Lightsource (SSRL) in Menlo Park, California, USA using the data acquisition program, XAS-Collect.[101] Cu K-edge data were collected on the biological XAS beamline (BL) 7-3 with the SPEAR storage ring containing 500 mA at 3.0 GeV. Beamline 7-3 utilizes a Si(220) double-crystal monochromator and a rhodium-coated vertically collimating mirror upstream of the monochromator, which achieves the appropriate harmonic rejection for the energy range by adjusting the mirror cutoff angle (i.e., to 12 keV for Cu). Samples were maintained at ∼10 K using a liquid helium flow cryostat during data collection and were also inclined at 45° to the incident X-ray beam as

https://dx.doi.org/10.1021/acs.inorgchem.0c01356
Inorg. Chem. XXXX, XXX, XXX−XXX

described above. Incident and transmitted X-rays were measured using nitrogen-filled gas ionization chambers with a sweeping voltage of 1.6 kV. Fluorescence spectra were collected by monitoring the Cu Kα fluorescence using a 30-element germanium detector[102] (Canberra Ltd., Meriden, CT, USA) oriented at 90° to the incident beam, with nickel filters and a Soller slit assembly to maintain detector count-rates within the pseudolinear regime. The monochromator energy was calibrated through reference to a standard Cu foil measured simultaneously with the sample. Specifically, the first energy inflection of the Cu foil was used to calibrate the spectrum energy to 8980.3 eV. Each data set is a collection of a minimum of 5 scans. To decrease the risk of photoreduction of Cu(II) compounds, samples were scanned at multiple positions on the same sample (i.e., using a 0.5 × 12 mm beam and 0.5 mm vertical movements) and near-edges of successive scans were compared for loss of the 1s → 3d transition, which is indicative of photoreduction.[62]

4.5. XAS Data Analysis. XAS data were analyzed using the EXAFSPAK suite of computer programs.[73] Specifically, XAS spectra were calibrated through reference to the internal Cu foil standard, and individual sweeps were averaged. Spectra were then baseline subtracted to remove contributions from scatter and other unwanted radiation, and a spline was fit to the data. The spline was then used to normalize near-edge spectra to 1 and to extract the EXAFS. The EXAFS region of the spectra was k^3-weighted, and the EXAFS Fourier transform was calculated employing Simpson's rule of integration to account for different k-space point spacing. Fourier transforms are phase-corrected for Cu−O backscattering.

4.6. Density Functional Theory Calculations. Density functional theory (DFT) calculations utilized Dmol^3 Materials Studio 7.0, with geometry optimization employing the generalized gradient approximation (GGA)[103] with Becke exchange[104] and Perdew[105] functionals. Optimization calculations used all-electron core treatment and were calculated *in vacuo* (i.e., without a solvent reaction field). Calculations used symmetry parameters to define the point group of Cu(II) 8HQ complexes. DFT calculations were spin unrestricted using the formal spin as the initial starting point. UV−visible spectra were calculated using time-dependent DFT (TD-DFT) employing the adiabatic local density approximation (ALDA)[106] and computing the 32 lowest excitation energies from the ground-state-optimized geometries.

4.7. EXAFS Curve-Fitting. Quantitative analyses utilized FEFF (ver. 8.25)[107,108] to calculate the *ab initio* theoretical phase and amplitude of energy-minimized molecular models from DFT calculations for use by the curve-fitting program OPT (a component of EXAFSPAK). The number (N) of each type of backscattering atom was not refined but was fit as an integer based on the parent model. Refinable parameters included the following: distance (R) between Cu and the backscattering atom, mean square deviation in R (Debye−Waller factor; σ^2), and the energy offset (ΔE_0) to the nominal threshold energy (9000 eV). As indicated, values for N were defined from the energy-minimized structures used to generate the multiple scattering model and were maintained as fixed integers throughout the fitting procedure. R parameters were fit as a group of linked paths; R values listed in Tables 2 and S3 with a standard error in parentheses were allowed to float within the refinement. The σ^2 values for each distance, R, were refined as a group for the entire energy minimized structural model. The fit error function F is defined as

$$F = \{\Sigma k^6(\chi_{calc} - \chi_{expt})^2/\Sigma\chi_{expt}^2\}^{1/2} \quad (1)$$

Noise contributions with frequencies higher than the longest bond length in the fit can be estimated as previously described.[109] Briefly, this was done by computing the product of the complex Cu−N phase-corrected discrete EXAFS Fourier transform with a half-Gaussian window function placed above the highest bond-length considered in the fit, which was 7.0 Å. The discrete Fourier transform contains all frequencies supported by the k-space data, extending to

$$R_{max} = \frac{2\pi}{\delta k} \quad (2)$$

where δk is the minimum k-space point separation. The back-transform of this was then computed and used to estimate F', employing eq 1. Fitting parameters for each best fit model are summarized in Table 2 and detailed in Table S4.

4.8. EPR Spectroscopy. ^{63}CuO (>99% ^{63}Cu, Isoflex, USA, San Francisco, CA) was dissolved by stirring it in conc. HCl. The conc. HCl was then evaporated to remove excess Cl^-, and the resultant brown solid was dissolved in diH_2O to a final concentration of 20 mM $^{63}CuCl_2$. For X-band EPR, 0.5 mol equiv of $^{63}CuCl_2$ were added to buffered 8HQ solutions. Exact concentrations are reported in the figure legend (Figure 6). Isotopically enriched ^{63}Cu was used to avoid broadening of resonance lines because of the different magnetic moments of naturally abundant isotopes (69% ^{63}Cu, g_n = 1.4840; 31% ^{65}Cu, g_n = 1.5900).

X-band EPR (~9.43 GHz) spectra were recorded on JEOL RE1X, JEOL JES-FA200, or Bruker EMX instruments equipped with TE_{011} cylindrical cavities or a Bruker ER 4122SHQE resonator. Typical spectrometer conditions were a 0.1 mT modulation amplitude, 5 mW applied microwave power, and a cooled-nitrogen temperature of approximately 121 K.

EPR powder line shape simulation used a modified version of the program QPOW.[110,111] ORCA (ver. 4.0.1.2.)[112,113] calculations of EPR parameters used a Becke exchange[104] and Perdew[105] functional with ZORA-def2-TZVP[114] and SARC/J[115] basis sets.

■ ASSOCIATED CONTENT

Supporting Information

The Supporting Information is available free of charge at https://pubs.acs.org/doi/10.1021/acs.inorgchem.0c01356.

Calculated log$P$ values; UV−visible absorption spectra; additional information on density functional theory calculations and geometry optimized structures; additional energy and intensity information for HERFD-XAS near edge spectra; experimental XAS photoreduction data; calculated EXAFS spectra and Fourier transforms; diagrams of linear and nonlinear multiple scattering paths; detailed EXAFS fitting parameters; and additional EPR spectra (PDF)

■ AUTHOR INFORMATION

Corresponding Authors

Kelly L. Summers − *Molecular and Environmental Sciences Group, Department of Geological Sciences and Department of Chemistry, University of Saskatchewan, Saskatoon, Saskatchewan S7N 5E2, Canada;* orcid.org/0000-0001-9185-5052; Email: kelly.summers@usask.ca

Ingrid J. Pickering − *Molecular and Environmental Sciences Group, Department of Geological Sciences, Department of Chemistry, and Toxicology Centre, University of Saskatchewan, Saskatoon, Saskatchewan S7N 5E2, Canada;* orcid.org/0000-0002-0936-2994; Email: ingrid.pickering@usask.ca

Graham N. George − *Molecular and Environmental Sciences Group, Department of Geological Sciences, Department of Chemistry, and Department of Anatomy and Cell Biology, University of Saskatchewan, Saskatoon, Saskatchewan S7N 5E2, Canada;* orcid.org/0000-0002-0420-7493; Email: graham.george@usask.ca

Authors

M. Jake Pushie − *Molecular and Environmental Sciences Group, Department of Geological Sciences, University of Saskatchewan, Saskatoon, Saskatchewan S7N 5E2, Canada;* orcid.org/0000-0001-7494-5427

George J. Sopasis − *Department of Chemistry, University of Adelaide, South Australia 5005, Australia*

https://dx.doi.org/10.1021/acs.inorgchem.0c01356
Inorg. Chem. XXXX, XXX, XXX−XXX

Ashley K. James − *Molecular and Environmental Sciences Group, Department of Geological Sciences, Department of Anatomy and Cell Biology, and Toxicology Centre, University of Saskatchewan, Saskatoon, Saskatchewan S7N 5E2, Canada*
Natalia V. Dolgova − *Molecular and Environmental Sciences Group, Department of Geological Sciences, University of Saskatchewan, Saskatoon, Saskatchewan S7N 5E2, Canada*
Dimosthenis Sokaras − *Stanford Synchrotron Radiation Lightsource, SLAC National Accelerator Laboratory, Stanford University, Menlo Park, California 94025, United States*
Thomas Kroll − *Stanford Synchrotron Radiation Lightsource, SLAC National Accelerator Laboratory, Stanford University, Menlo Park, California 94025, United States*
Hugh H. Harris − *Department of Chemistry, University of Adelaide, South Australia 5005, Australia;* orcid.org/0000-0002-3472-8628

Complete contact information is available at: https://pubs.acs.org/10.1021/acs.inorgchem.0c01356

Author Contributions

The manuscript was written through contributions of all authors. All authors have given approval to the final version of the manuscript.

Notes

The authors declare no competing financial interest.

■ ACKNOWLEDGMENTS

K.L.S gratefully acknowledges an Alexander Graham Bell Canadian Graduate Scholarship from the Natural Sciences and Engineering Research Council of Canada (NSERC) and support from the Canadian Institutes of Health Research (CIHR) Training Grant in Health Research Using Synchrotron Techniques (THRUST). K.L.S. also acknowledges a Michael Smith Foreign Study Supplement from NSERC. H.H.H. acknowledges financial support from the Australian Research Council (DP140100176). I.J.P and G.N.G are Canada Research Chairs and are supported by NSERC, the Saskatchewan Health Research Foundation (SHRF), a Canada Foundation for Innovation John Evans Leaders Fund award, and the University of Saskatchewan. XAS was carried out at the Stanford Synchrotron Radiation Lightsource (SSRL), SLAC National Accelerator Laboratory, which is funded by U.S. Department of Energy (DOE), Office of Science, Office of Basic Energy Sciences (DE-AC02-76SF00515). The SSRL Structural Molecular Biology Program is supported by the DOE Office of Biological and Environmental Research and by the National Institutes of Health and the National Institute of General Medical Sciences (P41GM103393). The contents of this publication are solely the responsibility of the authors and do not necessarily represent the official views of NIGMS or NIH. We would also like to acknowledge assistance from members of the Molecular and Environmental Sciences research group who provided assistance at SSRL beamline 7-3.

■ ABBREVIATIONS

8HQ, 8-hydroxyquinoline; MCQ, 5-chloro-7-iodo-8-hydroxy-2-methylquinoline; AI2Q, 5,7-diiodo-8-hydroxyquinoline-2-carboxaldehyde; MI2Q, 5,7-diiodo-8-hydroxy-2-methylquinoline; AC2Q, 5,7-dichloro-8-hydroxyquinoline-2-carboxaldehyde; Aβ, amyloid beta; AD, Alzheimer's disease; B2Q, 5,7-dibromo-8-hydroxyquinoline; CQ, clioquinol, 5-chloro-7-iodo-8hydroxyquinoline; EPR, electron paramagnetic resonance spectroscopy; EXAFS, extended X-ray absorption fine structure; FT, Fourier transform; HERFD-XAS, high-energy resolution fluorescence detected X-ray absorption spectroscopy; HD, Huntington's disease; I2Q, 5,7-diiodo-8-hydroxyquinoline; LMCT, ligand-to-metal charge transfer; M8Q, 2-methyl-8-hydroxyquinoline; MC2Q, 2-methyl-5,7-dichloro-8-hydroxyquinoline; NMR, nuclear magnetic resonance spectroscopy; PBT2, 5,7-dichloro-2-[(dimethylamino)methyl]-8-hydroxyquinoline; SMON, subacute myelo-optic neuropathy; XAS, X-ray absorption spectroscopy

■ REFERENCES

(1) Hollingshead, R. G. W. *Derivatives of oxine*; Butterworths Scientific Publications: London, 1956; Vol. *I*.
(2) Hollingshead, R. G. W. *Oxine*; Butterworths Scientific Publications: London, 1954; Vol. *I*.
(3) Welcher, F. J. Quinoline and quinoline derivatives. In *Organic Analytical Reagents*; D. Van Nostrand Company, Inc.: 1947; Vol. 3, pp 49.
(4) Wendlandt, W. W.; Horton, R. G. Differential thermal analysis of some metal chelates of 8-quinolinol and substituted 8-quinolinols. *Anal. Chem. (Washington, DC, U. S.)* **1962**, *34* (9), 1098−1101.
(5) Berg, V. R.; Kustenmacher, H. 5,7-dibrom-o(8)-oxychinolin, ein neues spezifisches reagens auf kupfer, eisen und titan in der quantitativen analyse. *Z. Anorg. Allg. Chem.* **1932**, *204*, 215−221.
(6) Berg, V. R. Über den einflub von substituenten auf die schwerloslichkeit und bestandigkeit von metallkomplexen der o(8)-oxychinolinderivate. *Z. Anorg. Allg. Chem.* **1932**, *204*, 208−214.
(7) Wendlandt, W. W. The thermal decomposition of some metal chelates of 5,7-diiodo-8-quinolinol. *Anal. Chim. Acta* **1956**, *15*, 533−537.
(8) Schaumburg, H.; Herskovitz, S. Copper deficiency myeloneuropathy: A clue to clioquinol-induced subacute myelo-optic neuropathy? *Neurology* **2008**, *71* (9), 622−623.
(9) Prachayasittikul, V.; Prachayasittikul, S.; Ruchirawat, S.; Prachayasittikul, V. 8-Hydroxyquinolines: A review of their metal chelating properties and medicinal applications. *Drug Des., Dev. Ther.* **2013**, *7*, 1157−1178.
(10) Hollingshead, R. G. W. The antibacterial and antifungal action of oxine, its derivatives and chelates. In *Oxine and Its Derivatives*; Butterworths Scientific Publications: London, 1956; Vol. *IV*, pp 1013−1058.
(11) Nakae, K.; Yamamoto, S.-I.; Shigematsu, I.; Kono, R. Relation between subacute myelo-optic neuropathy (S.M.O.N.) and clioquinol: Nationwide survey. *Lancet* **1973**, *301* (7796), 171−173.
(12) UN Department of Economic and Social Affairs. Clioquinol. *Consolidated List of Products Whose Consumption and/or Sale Have Been Banned, Withdrawn, Severely Restricted or Not Approved by Governments*; United Nations Digital Library: 2005; pp 89−91.
(13) Konagaya, M.; Matsumoto, A.; Takase, S.; Mizutani, T.; Sobue, G.; Konishi, T.; Hayabara, T.; Iwashita, H.; Ujihira, T.; Miyata, K.; Matsuoka, Y. Clinical analysis of longstanding subacute myelo-optico-neuropahty: Sequelae of clioquinol at 32 years after its ban. *J. Neurol. Sci.* **2004**, *218*, 85−90.
(14) Shaumburg, H. H., Clioquinol. In *Experimental and Clinical Neurotoxicology*, 2 ed.; Spencer, P. S., Schaumburg, H. H., Ludolph, A. C., Eds. Oxford University Press: Oxford, 2000; pp 397−400.
(15) Kaeser, H. E. Transient global amnesia due to clioquinol. *Acta Neurol Scand* **1984**, *70* (100), 175−179.
(16) Tamura, Z.; Yoshioka, M.; Imanari, T.; Fukaya, J.; Kusaka, J.; Samejima, K. Identification of green pigment and analysis of clioquinol in specimens from patients with subacute myelo-optic-neuropathy. *Clin. Chim. Acta* **1973**, *47*, 13−20.
(17) Tjälve, H. The aetiology of SMON may involve an interation between clioquinol and environmental metals. *Med. Hypotheses* **1984**, *15*, 293−299.
(18) Arbiser, J. L.; Kraeft, S.-K.; van Leeuwen, R.; Hurwitz, S. J.; Selig, M.; Dickersin, G. R.; Flint, A.; Byers, H. R.; Chen, L. B.

Clioquinol-zinc chelate: A candidate causative agent of subacute myelo-optic neuropathy. *Mol. Med.* **1998**, *4* (10), 665−670.
(19) Kumar, N.; Gross, J. B.; Ahlskog, J. E. Copper deficiency myelopathy produces a clinical picture like subacute combined degeneration. *Neurology* **2004**, *63* (1), 33−39.
(20) Berggren, L.; Hansson, O. Absorption of intestinal antiseptics derived from 8-hydroxyquinolines. *Clin. Pharmacol. Ther.* **1968**, *9* (1), 67−70.
(21) Cherny, R.; Atwood, C. G.; Xilinas, M.; Gray, D. N.; Jones, W. D.; McLean, C. A.; Barnham, K. J.; Volitakis, I.; Fraser, F. W.; Kim, Y.; Huang, X.; Goldstein, L. E.; Moir, R. D.; Lim, J. T.; Beyreuther, K.; Zheng, H.; Tanzi, R. E.; Masters, C. L.; Bush, A. I. Treatment with a copper-zinc chelator markedly and rapidly inhibits b-amyloid accumulation in Alzheimer's disease transgenic mice. *Neuron* **2001**, *30* (3), 665−676.
(22) Adlard, P. A.; Cherny, R. A.; Finkelstein, D. I.; Gautier, E.; Robb, E.; Cortes, M.; Volitakis, I.; Liu, X.; Smith, J. P.; Perez, K.; Laughton, K.; Li, Q.-X.; Charman, S. A.; Nicolazzo, J. A.; Wilkins, S.; Deleva, K.; Lynch, T.; Kok, G.; Ritchie, C. W.; Tanzi, R. E.; Cappai, R.; Masters, C. L.; Barnham, K. J.; Bush, A. I. Rapid restoration of cognition in Alzheimer's transgenic mice with 8-hydroxyquinoline analogs is associated with decreased interstitial Aβ. *Neuron* **2008**, *59* (1), 43−55.
(23) Ritchie, C. W.; Bush, A. I.; Mackinnon, A.; Macfarlane, S.; Mastwyk, M.; MacGregor, L.; Kiers, L.; Cherny, R.; Li, Q. X.; Tammer, A.; Carrington, D.; Mavros, C.; Volitakis, I.; Xilinas, M.; Ames, D.; Davis, S.; Beyreuther, K.; Tanzi, R. E.; Masters, C. L. Metal-protein attenuation with iodochlorhydroxyquin (clioquinol) targeting Ab amyloid deposition and toxicity in Alzheimer disease - A pilot phase 2 clinical trial. *Arch. Neurol.* **2003**, *60* (12), 1685−1691.
(24) Ibach, B.; Haen, E.; Marienhagen, J.; Hajak, G. Clioquinol treatment in familiar early onset Alzheimer's disease: A case report. *Pharmacopsychiatry* **2005**, *38* (4), 178−179.
(25) Lannfelt, L.; Blennow, K.; Zetterberg, H.; Batsman, S.; Ames, D.; Harrison, J.; Masters, C. L.; Targum, S.; Bush, A. I.; Murdoch, R.; Wilson, J.; Ritchie, C. W. Safety, efficacy, and biomarker findings of PBT2 in targeting Ab as a modifying therapy for Alzheimer's disease: A phase IIa, double-blind, randomised, placebo-controlled trial. *Lancet Neurol.* **2008**, *7* (9), 779−786.
(26) Faux, N. G.; Ritchie, C. W.; Gunn, A.; Rembach, A.; Tsatsanis, A.; Bedo, J.; Harrison, J.; Lannfelt, L.; Blennow, K.; Zetterberg, H.; Ingelsson, M.; Masters, C. L.; Tanzi, R. E.; Cummings, J. L.; Herd, C. M.; Bush, A. I. PBT2 rapidly improves cognition in Alzheimer's disease: Additional phase II analyses. *J. Alzheimer's Dis.* **2010**, *20* (2), 509−516.
(27) Barnham, K. J.; Bush, A. I. Biological metals and metal-targeting compounds in major neurodegenerative diseases. *Chem. Soc. Rev.* **2014**, *43*, 6727−6749.
(28) Walker, F. O. Huntington's disease. *Lancet* **2007**, *369* (9557), 218−228.
(29) Nguyen, T.; Hamby, A.; Massa, S. M. Clioquinol down-regulates mutant huntingtin expression *in vitro* and mitigates pathology in a Huntington's disease mouse model. *Proc. Natl. Acad. Sci. U. S. A.* **2005**, *102* (33), 11840−11845.
(30) Cherny, R.; Ayton, S.; Finkelstein, D. I.; Bush, A. I.; McColl, G.; Massa, S. M. PBT2 reduces toxicity in a *C. elegans* model of polyQ aggregation and extends lifespan, reduces striatal atrophy and inproves motor performance in the R6/2 mouse model of Huntington's disease. *J. Huntington's Dis.* **2012**, *1*, 211−219.
(31) Prana Biotechnology Limited. Prana Announces Successful Phase 2 Results in Huntington Disease Trial. Prana Biotechnology Limited: 2014; https://alteritytherapeutics.com/investor-centre/news/2014/02/18/prana-announces-successful-phase-2-results-huntington-disease-trial/ (accessed 2020).
(32) Huntington Study Group Reach2HD Investigators. Safety, tolerability, and efficacy of PBT2 in Huntington's disease: a phase 2, randomised, double-blind, placebo-controlled trial. *Lancet Neurol.* **2015**, *14* (1), 39−47.
(33) Leanderson, P.; Tagesson, C. Iron bound to the lipophilic iron chelator, 8-hydroxyquinoline, causes DNA strand breakage in cultured lung cells. *Carcinogenesis* **1996**, *17* (3), 545−550.
(34) Liu, Y.-C.; Wei, J.-H.; Chen, Z.-F.; Liu, M.; Gu, Y.-Q.; Huang, K.-B.; Li, Z.-Q.; Liang, H. The antitumor activity of zinc(II) and copper(II) complexes with 5,7-dihalo-substituted-8-quinolinoline. *Eur. J. Med. Chem.* **2013**, *69*, 554−563.
(35) Moon, H.; Han, S.; Park, H.; Choe, J. Crystal structures of human FIH-1 in complex with quinol family inhibitors. *Mol. Cells* **2010**, *29* (5), 471−474.
(36) Park, M. H.; Lee, S. J.; Byun, H. R.; Kim, Y.; Oh, Y. J.; Koh, J.-Y.; Hwang, J. J. Clioquinol induces autophagy in cultured astrocytes and neurons by acting as a zinc ionophore. *Neurobiol. Dis.* **2011**, *42* (3), 242−251.
(37) Nitzan, Y. B.; Sekler, I.; Frederickson, C. J.; Coulter, D. A.; Balaji, R. V.; Liang, S. L.; Margulis, A.; Hershfinkel, M.; Silverman, W. F. Clioquinol effects on tissue chelatable zinc in mice. *J. Mol. Med.* **2003**, *81* (10), 637−644.
(38) White, A. R.; Du, T.; Laughton, K. M.; Volitakis, I.; Sharples, R. A.; Xilinas, M. E.; Hoke, D. E.; Holsinger, R. M. D.; Evin, G.; Cherny, R. A.; Hill, A. F.; Barnham, K. J.; Li, Q.-X.; Bush, A. I.; Masters, C. L. Degradation of the Alzheimer disease amyloid β-peptide by metal-dependent up-regulation of metalloprotease activity. *J. Biol. Chem.* **2006**, *281*, 17670−17680.
(39) Ding, W.-Q.; Liu, B.; Vaught, J. L.; Yamauchi, H.; Lind, S. E. Anticancer activity of the antibiotic clioquinol. *Cancer Res.* **2005**, *65*, 3389−3395.
(40) Crouch, P. J.; Savva, M. S.; Hung, L. W.; Donnelly, P. S.; Mot, A. I.; Parker, S. J.; Greenough, M. A.; Volitakis, I.; Adlard, P. A.; Cherny, R.; Masters, C. L.; Bush, A. I.; Barnham, K. J.; White, A. R. The Alzheimer's therapeutic PBT2 promotes amyloid-beta degredation and GSK-3 phosphorylation via a metal chaperone activity. *J. Neurochem.* **2011**, *119* (1), 220−230.
(41) Tardito, S.; Barilli, A.; Bassanetti, I.; Tegoni, M.; Bussolati, O.; Franchi-Gazzola, R.; Mucchino, C.; Marchio, L. Copper-dependent cytotoxicity of 8-hydroxyquinoline derivatives correlates with their hydrophobicity and does not require caspase activation. *J. Med. Chem.* **2012**, *55*, 10448−10459.
(42) D. Schimmer, A. Clioquinol - A novel copper-dependent and independent proteasome inhibitor. *Curr. Cancer Drug Targets* **2011**, *11*, 325−331.
(43) Yu, H.; Zhou, Y.; Lind, S. E.; Ding, W.-Q. Clioquinol targets zinc to lysosomes in human cancer cells. *Biochem. J.* **2009**, *417*, 133−139.
(44) Denoyer, D.; Pearson, H. B.; Clatworthy, S. A. S.; Smith, Z. M.; Francis, P. S.; Llanos, R. M.; Volitakis, I.; Phillips, W. A.; Meggyesy, P. M.; Masaldan, S.; Cater, M. A. Copper as a target for prostate cancer therapeutics: Copper-ionophore pharmacology and altering systemic copper distribution. *Oncotarget* **2016**, *7* (24), 37064−37080.
(45) Portnoy, B.; Molokhia, M. Acrodermatitis enteropathica treated by zinc. *Br. J. Dermatol.* **1974**, *91*, 701−703.
(46) Geiser, J.; De Lisle, R. C.; Finkelstein, D. I.; Adlard, P. A.; Bush, A. I.; Andrews, G. K. Clioquinol synergistically augments rescue by zinc supplementation in a mouse model of acrodermatitis enteropathica. *PLoS One* **2013**, *8* (8), No. e72543.
(47) Hägermark, Ö.; Wahlberg, J. E.; Germanis, M. Determination of oxyquinoline concentrations in plasma in a patient treated for acrodermatitis enteropathica - An aid in therapeutic control. *Dermatology* **2004**, *149*, 29−38.
(48) Sgarlata, C.; Arena, G.; Bonomo, R. P.; Giuffrida, A.; Tabbi, G. Simple and mixed complexes of copper(II) with 8-hydroxyquinoline derivatives and amino acids: Characterization in solution and potential biological implications. *J. Inorg. Biochem.* **2018**, *180*, 89−100.
(49) Nguyen, M.; Vendier, L.; Stigliani, J.-L.; Meunier, B.; Robert, A. Structures of the copper and zinc complexes of PBT2, a chelating agent evaluated as potential drug for neurodegenerative diseases. *Eur. J. Inorg. Chem.* **2017**, *2017* (2017), 600−608.

https://dx.doi.org/10.1021/acs.inorgchem.0c01356
Inorg. Chem. XXXX, XXX, XXX−XXX

(50) Albert, A.; Gibson, M. I.; Rubbo, S. D. The influence of chemical constitution on anti-bacterial activity. Part VI: The bactericidal action of 8-hydroxyquinoline (oxine). *Br. J. Exp. Pathol.* **1953**, *34* (2), 119−130.
(51) Budimir, A.; Humbert, N.; Elhabiri, M.; Osinska, I.; Biruš, M.; Albrecht-Gary, A.-M. Hydroxyquinoline based binders: Promising ligands for chemotherapy. *J. Inorg. Biochem.* **2011**, *105* (3), 490−496.
(52) Phillips, J. P. The reactions of 8-quinolinol. *Chem. Rev.* **1956**, *56* (2), 271−297.
(53) Di Vaira, M.; Bazzicalupi, C.; Orioli, P.; Messori, L.; Bruni, B.; Zatta, P. Clioquinol, a drug for Alzheimer's disease specifically interfering with brain metal metabolism: Structural characterization of its zinc(II) and copper(II) complexes. *Inorg. Chem.* **2004**, *43*, 3795−3797.
(54) Chen, D.; Cui, Q. C.; Yang, H.; Barrea, R. A.; Sarkar, F. H.; Sheng, S.; Yan, B.; Reddy, G. P. V.; Dou, Q. P. Clioquinol, a therapeutic agent for Alzheimer's disease, has proteasome-inhibitory, androgen receptor-suppressing, apoptosis-inducing, and antitumor activities in human prostate cancer cells and xenografts. *Cancer Res.* **2007**, *67*, 1636−1644.
(55) Pushie, M. J.; Nienaber, K. H.; Summers, K. L.; Cotelesage, J. J. H.; Ponomarenko, O.; Nichol, H. K.; Pickering, I. J.; George, G. N. The solution structure of the copper clioquinol complex. *J. Inorg. Biochem.* **2014**, *133*, 50−56.
(56) Anjaneyulu, Y.; Pisipati, V. G. K. M.; Rao, N. V. S.; Murthy, L. N.; Prao, R.; Swamy, R. Y. ESR studies of halogen-substituted 8-hydroxyginoline copper II complexes. *Indian J. Pure Appl. Phys.* **1986**, *24*, 309−311.
(57) Palenik, G. J. The structure of coordination compounds. II. The crystal and molecular structure of the b form of anhydrous copper 8-hydroxyquinolinate. *Acta Crystallogr.* **1964**, *17*, 687−695.
(58) Hoy, R. C.; Morriss, R. H. The crystal structure of the [alpha] form of anhydrous copper 8-hydroxyquinolinate. *Acta Crystallogr.* **1967**, *22* (4), 476−482.
(59) Marino, T.; Pavelka, M.; Toscano, M.; Russo, N. Structural and binding properties of metal ion chelators relevant to Alzheimer's disease. A theoretical investigation. *Int. J. Quantum Chem.* **2012**, *112*, 2109−2114.
(60) Yang, L.; Powell, D. R.; Houser, R. P. Structural variation in copper(I) complexes with pyridylmethylamide ligands: Structural analysis with a new four-coordinate geometry index, τ4. *Dalton T.* **2007**, No. 9, 955−964.
(61) Okuniewski, A.; Rosiak, D.; Chojnacki, J.; Becker, B. Coordination polymers and molecular structures among complexes of mercury(II) halides with selected 1-benzoylthioureas. *Polyhedron* **2015**, *90*, 47−57.
(62) George, G. N.; Pickering, I. J.; Pushie, M. J.; Nienaber, K.; Hackett, M. J.; Ascone, I.; Hedman, B.; Hodgson, K. O.; Aitken, J. B.; Levina, A.; Glover, C.; Lay, P. A. X-ray-induced photo-chemistry and X-ray absorption spectroscopy of biological samples. *J. Synchrotron Radiat.* **2012**, *19*, 875−886.
(63) Summers, K. L.; Schilling, K. M.; Roseman, G.; Markham, K. A.; Dolgova, N. V.; Kroll, T.; Sokaras, D.; Millhauser, G. L.; Pickering, I. J.; George, G. N. X-ray absorption spectroscopy investigations of copper(II) coordination in the human amyloid β peptide. *Inorg. Chem.* **2019**, *58* (9), 6294−6311.
(64) Hämäläinen, K.; Siddons, D. P.; Hastings, J. B.; Berman, L. E. Elimination of the inner-shell lifetime broadening in X-ray absorption spectroscopy. *Phys. Rev. Lett.* **1991**, *67* (20), 2850−2853.
(65) Kosugi, N.; Yokoyama, T.; Asakura, K.; Kuroda, H. Polarized Cu K-edge XANES of square planar $CuCl_4^{2-}$ ion. Experimental and theoretical evidence for shake-down phenomena. *Chem. Phys.* **1984**, *91* (2), 249−256.
(66) Pickering, I. J.; George, G. N. Polarized X-ray absorption spectroscopy of cupric chloride dihydrate. *Inorg. Chem.* **1995**, *34* (12), 3142−3152.
(67) Kanamaru, F.; Ogawa, K.; Nitta, I. The crystal structures of metal 8-hydroxyquinolinate. I. Copper 8-hydroxyquinolinate. *Bull. Chem. Soc. Jpn.* **1963**, *36* (4), 422−427.
(68) Petit, S.; Coquerel, G.; Perez, G.; Louer, D.; Louer, M. Synthesis, characterization and *ab initio* structure determination from powder diffraction data of a new X' form of anhydrous copper(II) 8-hydroxyquinolinate doped with amine. Modeling of the polymorphic transformation to the stable anhydrous *b''* form. *Chem. Mater.* **1994**, *6* (2), 116−121.
(69) Low, K.-H.; Xu, Z.-X.; Xiang, H.-F.; Chui, S. S.-Y.; Roy, V. A. L.; Che, C.-M. Bis(5,7-dimethyl-8-hydroxyquinolinato)platinum(II) complex for efficient organic heterojunction solar cells. *Chem. - Asian J.* **2011**, *6* (12), 3223−3229.
(70) Lindner, B. D.; Paulus, F.; Appleton, A. L.; Schaffroth, M.; Engelhart, J. U.; Schelkle, K. M.; Tverskoy, O.; Rominger, F.; Hamburger, M.; Bunz, U. H. F. Electron-transporting phenazinothiadiazoles with engineered microstructure. *J. Mater. Chem. C* **2014**, *2* (45), 9609−9612.
(71) Sambiagio, C.; Munday, R. H.; Marsden, S. P.; Blacker, A. J.; McGowan, P. C. Picolinamides as effective ligands for copper-catalysed aryl ether formation: Structure−activity relationships, substrate scope and mechanistic investigations. *Chem. - Eur. J.* **2014**, *20* (52), 17606−17615.
(72) Banik, R.; Roy, S.; Bauza, A.; Frontera, A.; Rodríguez-Diéguez, A.; Salas, J. M.; Kirillov, A. M.; Chowdhury, S.; Das, S. K.; Das, S. Supramolecular interactions through lone pair(lp)−π and hydrogen bonding in cobalt(III) and manganese(II) derivatives of N, N′-dimethylvioluric acid: A combined experimental and theoretical study. *Inorg. Chim. Acta* **2015**, *435*, 178−186.
(73) George, G. N. EXAFSPAK, 2001. Available from: ssrl.slac.stanford.edu/exafspak.html.
(74) Aragoni, M. C.; Arca, M.; Bencini, A.; Blake, A. J.; Caltagirone, C.; De Filippo, G.; Devillanova, F. A.; Garau, A.; Gelbrich, T.; Hursthouse, M. B.; Isaia, F.; Lippolis, V.; Mameli, M.; Mariani, P.; Valtancoli, B.; Wilson, C. Tuning the selectivity/specificity of fluorescent metal ion sensors based on N2S2 pyridine-containing macrocyclic ligands by changing the fluorogenic subunit: Spectrofluorimetric and metal ion binding studies. *Inorg. Chem.* **2007**, *46* (11), 4548−4559.
(75) Murray-Rust, P.; Wright, J. D. Molecular complexes. Part VIII. The crystal structure of the 1:2 complex of bis-8-hydroxyquinolinatocopper(II) and 1,2,4,5-tetracyanobenzene. *J. Chem. Soc. A* **1968**, No. 0, 247−253.
(76) Pu, Y.-M.; Ku, Y.-Y.; Grieme, T.; Henry, R.; Bhatia, A. V. An efficient copper-catalyzed N-arylation of pyridazinones with a structurally well-defined copper complex. *Tetrahedron Lett.* **2006**, *47*, 149−153.
(77) Shoja, M.; Gershon, H.; Clark, D. D. Crystal structure of bis(7-nitro-8-quinolinolato)copper(II), $CuC_{18}H_{10}O_6N_4$. *Zeitschrift für Kristallographie* **2000**, *215*, 273−274.
(78) Zhang, F.; Zhang, Y.-Y.; Gao, X.; Zhang, X.-D.; Li, Y.-Z.; Chen, H.-L.; Liu, Q.-T. CCDC 627891: Experimental crystal structure determination. CCDC: 2007, DOI: 10.5517/ccp2ckn.
(79) Zhang, W.-L.; Liu, Y.-Y.; Ma, J.-F.; Jiang, H.; Yang, J.; Ping, G.-J. Fine tuning of the Cu(II)-bis(imidazole) networks by changing sulfonate anions. *Cryst. Growth Des.* **2008**, *8* (4), 1250−1256.
(80) Shoja, M.; Gershon, H.; Bray, D.; Clarke, D. D. Crystal structures of copper(II) complexes of some 2-methyl-8-quinolinols and implications for their antifungal activity. *Monatsh. Chem.* **1998**, *129*, 843−853.
(81) Barilli, A.; Atzeri, C.; Bassanetti, I.; Ingoglia, F.; Dall'Asta, V.; Bussolati, O.; Maffini, M.; Mucchino, C.; Marchiò, L. Oxidative stress induced by copper and iron complexes with 8-hydroxyquinoline derivatives causes paraptotic death of HeLa cancer cells. *Mol. Pharmaceutics* **2014**, *11*, 1151−1163.
(82) Machura, B.; Świtlicka, A.; Mroziński, J.; Kłak, J.; Kruszynski, R.; Kusz, J.; Tabak, D. Synthesis, spectroscopic characterization, X-ray structure and magnetic properties of $[Cu(hmquin\text{-}7\text{-}COOH)_2(MeOH)]$ complex. *Polyhedron* **2009**, *28*, 3774−3780.
(83) Courcot, B.; Firley, D.; Fraisse, B.; Becker, P.; Gillet, J.-M.; Pattison, P.; Chernyshov, D.; Sghaier, M.; Zouhiri, F.; Desmaële, D.; d'Angelo, J.; Bonhomme, F.; Geiger, S.; Ghermani, N. E. Crystal and

https://dx.doi.org/10.1021/acs.inorgchem.0c01356
Inorg. Chem. XXXX, XXX, XXX−XXX

electronic structures of magnesium(II), copper(II), and mixed magnesium(II)-copper(II) complexes of the quinoline half styrylquinoline-type HIV-1 integrase inhibitors. *J. Phys. Chem. B* **2007**, *111*, 6042−6050.
(84) Itoh, K.; Tanaka, J.-I.; Setsune, J.-I.; Eda, K. Crystal structure of bis(2-diethoxycarbonylethanyl-8-hydroxyquinolinato-*N*,*O*)Cu(II). *Anal. Sci.: X-Ray Struct. Anal. Online* **2006**, *22*, 59−60.
(85) Yuan, G.; Rong, L.; Yue, C.; Wei, X. Supramolecular assembly of two two-folded helical structures based on 2-substituted 8-hydroxyquinoline complexes. *Inorg. Chem. Commun.* **2013**, *33*, 19−24.
(86) Kokoszka, G. F.; Allen, H. C.; Gordon, G. Electron paramagnetic resonance spectrum of bis-8-hydroxyquinolate copper-(II) dihydrate. *J. Chem. Phys.* **1965**, *42*, 3730−3731.
(87) Gersmann, H. R.; Swalen, J. D. Electron paramagnetic resonance spectra of copper complexes. *J. Chem. Phys.* **1962**, *36* (12), 3221−3233.
(88) Anjaneyulu, Y.; Pisipati, V. G. K. M.; Rao, N. V. S.; Murthy, L. N.; Prabhakara Rao, R. ESR studies of ternary complexes of copper(II) with acetylacetone and substituted 8-hydroxyquinolines. *Indian J. Pure Appl. Phys.* **1986**, *24*, 355−357.
(89) Cozar, I. B.; Szabo, L.; Mogonea, L.; Cozar, O.; David, L. EPR investigation of two Cu(II) complexes with low symmetry. *J. Optoelectron. Adv. M.* **2010**, *12* (8), 1799−1804.
(90) Yordanov, N. D.; Stankova, M.; Shopov, D. EPR study of bis(8-quinolinethiolato)copper(II) and bis(8-quinolinolato)copper(II) complexes. *Chem. Phys. Lett.* **1976**, *39* (1), 174−176.
(91) Horowitz, A. A. J.; Pryce, M. H. L.; Morton, K. W. On the hyperfine structure of paramagnetic resonance: The *s*-electron effect. *Proc. R. Soc. London, Ser. A* **1955**, *230*, 169−187.
(92) McGarvey, B. R. The isotropic hyperfine interaction. *J. Phys. Chem.* **1967**, *71* (1), 51.
(93) Allen, H. C.; Scullane, M. I. The isotropic hyperfine interaction in some tetradentate Schiff-base complexes of copper(II). *J. Coord. Chem.* **1978**, *8* (2), 93−98.
(94) Yordanov, N. D.; Alexiev, V. An EPR study of the CuL2′ CuL2" interactions in solution. *Bulgarian Academy of Sciences* **1983**, *2*, 214−223.
(95) Froncisz, W.; Hyde, J. S. Broadening by strains of lines in the g-parallel region of Cu^{2+} EPR spectra. *J. Chem. Phys.* **1980**, *73* (1), 3123−3131.
(96) Bakewell, C.; Platel, R. H.; Cary, S. K.; Hubbard, S. M.; Roaf, J. M.; Levine, A. C.; White, A. J. P.; Long, N. J.; Haaf, M.; Williams, C. K. Bis(8-quinolinolato)aluminium ethyl complexes: Iso-selective initiators for *rac*-lactide polymerization. *Organometallics* **2012**, *31*, 4729−4736.
(97) Basak, A.; Abouelhassan, Y.; Norwood, V. M., IV; Bai, F.; Nguyen, M. T.; Jin, S.; Huigens, R. W., III Synthetically tuning the 2-position of halogenated quinolines: Optimizing antibacterial and biofilm eradication activities via alkylation and reductive amination pathways. *Chem. - Eur. J.* **2016**, *22* (27), 9181−9189.
(98) Zhang, W.; Huang, D.; Huang, M.; Huang, J.; Wang, D.; Liu, X.; Nguyen, M.; Vendier, L.; Mazeres, S.; Robert, A.; Liu, Y.; Meunier, B. Preparation of tetradentate copper chelators as potential anti-Alzheimer agents. *ChemMedChem* **2018**, *13*, 684−704.
(99) Sokaras, D.; Weng, T.-C.; Nordlund, D.; Alonso-Mori, R.; Velikov, P.; Wenger, D.; Garachtchenko, A.; George, M.; Borzenets, V.; Johnson, B.; Rabedeau, T.; Bergmann, U. A seven-crystal Johann-type hard X-ray spectrometer at the Stanford Synchrotron Radiation Lightsource. *Rev. Sci. Instrum.* **2013**, *84* (5), 053102.
(100) George, G. N.; Garrett, R. M.; Prince, R. C.; Rajagopalan, K. V. The molybdenum site of sulfite oxidase: A comparison of wildtype and the cysteine 207 to serine mutant using X-ray absorption spectroscopy. *J. Am. Chem. Soc.* **1996**, *118*, 8588−8592.
(101) George, M. J. XAS-Collect: A computer program for X-ray absorption spectroscopic data acquisition. *J. Synchrotron Radiat.* **2000**, *7* (4), 283−286.
(102) Cramer, S. P.; Tench, O.; Yocum, M.; George, G. N. A 13-element Ge detector for fluorescence EXAFS. *Nucl. Instrum. Methods Phys. Res., Sect. A* **1988**, *266* (1−3), 586−591.
(103) Patton, D.; Pederson, M.; Porezag, D. The Generalized-Gradient Approximation to density functional theory and bonding. In *Frontiers in Materials Modelling and Design*; Kumar, V., Sengupta, S., Raj, B., Eds.; Springer: 1998; pp 37−50.
(104) Becke, A. D. A multicenter numerical integration scheme for polyatomic molecules. *J. Chem. Phys.* **1988**, *88*, 2547−2253.
(105) Perdew, J. P.; Wang, Y. Accurate and simple analytic representation of the electron-gas correlation energy. *Phys. Rev. B: Condens. Matter Mater. Phys.* **1992**, *45* (23), 13244−13249.
(106) Baer, R. Non-adiabatic couplings by time-dependent density functional theory. *Chem. Phys. Lett.* **2002**, *364*, 75−79.
(107) Mustre de Leon, J.; Rehr, J. J.; Zabinsky, S. I.; Albers, R. C. *Ab initio* curved-wave X-ray-absorption fine structure. *Phys. Rev. B: Condens. Matter Mater. Phys.* **1991**, *44* (9), 4146−4156.
(108) Rehr, J. J.; Mustre de Leon, J.; Zabinsky, S. I.; Albers, R. C. Theoretical X-ray absorption fine structure standards. *J. Am. Chem. Soc.* **1991**, *113* (14), 5135−5140.
(109) Pushie, M. J.; Cotelesage, J. J. H.; Lyashenko, G.; Hille, R.; George, G. N. X-ray absorption spectroscopy of a quantitatively Mo(V) dimethyl sulfoxide reductase species. *Inorg. Chem.* **2013**, *52* (6), 2830−2837.
(110) Nilges, M. J. *Electron paramagnetic resonance studies of low symmetry nickel(I) and molybdenum(V) complexes*. Ph.D. dissertation, University of Illinois, Urbana, IL, 1979.
(111) Maurice, A. M. *Acquisition of anisotropic information by computational analysis of isotropic EPR spectra*. Ph.D. dissertation. University of Illinois, Urbana, IL, 1980.
(112) Neese, F. The ORCA program system. *Wiley Interdiscip. Rev.: Comput. Mol. Sci.* **2012**, *2*, 73−78.
(113) Neese, F. Software update: The ORCA program system, version 4.0. *Wiley Interdiscip. Rev.: Comput. Mol. Sci.* **2018**, *8* (1), No. e1327.
(114) Weigend, F.; Ahlrichs, R. Balanced basis sets of split valence, triple zeta valence and quadruple zeta valence quality for H to Rn: Design and assessment of accuracy. *Phys. Chem. Chem. Phys.* **2005**, *7* (18), 3297−3305.
(115) Weigend, F. Accurate Coulomb-fitting basis sets for H to Rn. *Phys. Chem. Chem. Phys.* **2006**, *8* (9), 1057−1065.

https://dx.doi.org/10.1021/acs.inorgchem.0c01356
Inorg. Chem. XXXX, XXX, XXX−XXX